Title
MICROSTRUCTURE-MECHANICAL PROPERTY RELATIONSHIPS OF DUAL-PHASE STEEL WIRE

Author
Nakagawa, A.H.

Publication Date
1983-12-01

Lawrence Berkeley Laboratory
UNIVERSITY OF CALIFORNIA

Materials & Molecular Research Division

MICROSTRUCTURE-MECHANICAL PROPERTY RELATIONSHIPS OF DUAL-PHASE STEEL WIRE

A.H. Nakagawa
(Ph.D. Thesis)

December 1983

Prepared for the U.S. Department of Energy under Contract DE-AC03-76SF00098

DISCLAIMER

LBL-17099

MICROSTUCTURE-MECHANICAL PROPERTY RELATIONSHIPS OF DUAL-PHASE STEEL WIRE

Alvin Hisao Nakagawa
(Ph.D. Thesis)

Lawrence Berkeley Laboratory
University of California
Berkeley, California 94720

December 1983

This work was supported by the Director, Office of Energy Research, Office of Basic Energy Sciences, Division of Materials Sciences of the U.S. Department of Energy under Contract Number DE-AC03-76SF00098.

MICROSTRUCTURE-MECHANICAL PROPERTY RELATIONSHIPS OF DUAL-PHASE STEEL WIRE

Alvin Hisao Nakagawa

Ph.D.

Dept. of Materials Science and Mineral Engineering

Sponsor: U. S. Department of Energy

Gareth Thomas

Professor Gareth Thomas
Chairman of Committee

ABSTRACT

This thesis is concerned with the first (to the author's knowledge) attempts to utilize the properties of low carbon dual-phase steels to produce high strength wire as an alternative to existing practice using pearlitic medium to high carbon steels. This goal to design a dual-phase steel suitable for drawing into high strength wire necessitated a study of the relationships between the microstructure and properties of undrawn rod and rod drawn into wire, and of the deformation of dual-phase steel at large strains.

Dual-phase steel was selected for this study because of its pronounced strain hardening rate and superior formability. These properties permit dual-phase steel to be drawn to large strains and high strengths. The alloy composition and processing are

generally quite simple and they can be varied to produce a wide range of structures and mechanical properties to fit specific applications.

Dual-phase microstructures of several different martensite volume fractions, particle shapes, particle sizes, carbon contents and crystallographic relations with the ferrite matrix were studied. It was found that good mechanical properties could be obtained in wire drawn from dual-phase steel. The most promising steel was the Fe-2Si-0.1C alloy given a double heat treatment consisting of austenitizing and quenching to martensite, followed by two phase annealing at 950 C and quenching. This steel could be drawn to a true strain of 6.1 without intermediate annealing. It is recommended that a lower carbon content of 0.06 to 0.08 wt.% be used to lower the carbon content in the martensite, thereby reducing the amount of voids that form during drawing. Stress relief after wire drawing resulted in a substantial increase in the ductility of the wire. The effects of various other factors such as alloying, quench speed, drawing schedule and drawing speed on the structure and mechanical properties of the wire are discussed.

ACKNOWLEDGEMENTS

The author extends his sincere gratitude to Professor Gareth Thomas for the support and guidance provided during and beyond the course of this investigation.

Deepest thanks are also due to Dr. R. M. Fisher of United States Steel Corporation for his valuable discussions and advice. The time and effort expended by Professor S. Kobayashi and Dr. R. M. Fisher in reviewing this manuscript is gratefully acknowledged.

The author would like to thank Professor N. J. Kim, Dr. J. J. Rayment, and other former and present colleagues for the advice, assistance, and friendship necessary to complete graduate study. The technical assistance provided by the support staff of the Materials and Molecular Research Division of the Lawrence Berkeley Laboratory is acknowledged. Thanks are due in particular to J. Holthuis and W. Wong. Sandia National Laboratories, Albuquerque, NM and Nippon Kokan K. K. graciously supplied the alloys used in this investigation.

Finally, the author is grateful for the love and encouragement extended by his family, especially by his wife, Cheryl who was always there to provide boundless love, and spiritual as well as technical support during the ups and downs of graduate study.

This work was supported by the Director, Office of Energy Research, Office of Basic Energy Sciences, Division of Materials Sciences of the U. S. Department of Energy under Contract No. DE-AC03-76SF00098.

MICROSTRUCTURE-MECHANICAL PROPERTY RELATIONSHIPS OF DUAL-PHASE STEEL WIRE

CONTENTS

1. INTRODUCTION

Two of the many requirements for automobile sheet steels are high strength and good formability. The high strength permits the use of thinner gauge sheet resulting in lighter and more fuel efficient automobiles, and the often conflicting requirement of good formability is necessary if the steel is to be stamped into the complex shapes of automobile parts. One of the steels recently designed to meet these requirements is a high strength, low alloy (HSLA) steel known as dual-phase steel [1-3]. Since its introduction, considerable research effort has been directed towards understanding and improving this steel as reported at five symposia on the subject [4-8].

The basis of dual-phase steel is that of a composite. Despite the name "dual-phase", this steel may contain three or more phases. The matrix is usually soft ductile ferrite. The strengthening phase(s), which comprises 10 to 40 volume percent, is mainly hard strong martensite but may contain small amounts of bainite or retained austenite. However, in novel dual-phase steels developed by Kim [9] and Bangaru [10], the second phase is made up entirely of bainite or retained austenite respectively. When the second phase is martensitic, the preferred structure is dislocated lath martensite separated by thin films of retained austenite. This type of martensite substructure has been shown previously to be beneficial for good strength and toughness in martensitic steels [11,12] as well as in ferritic-martensitic steels [13,14].

The dual-phase microstructure can be produced by continuous annealing [1] or batch annealing [2,3] a ferrite-pearlite hot rolled steel in the intercritical ($\alpha + \gamma$) region for a short period of time followed by cooling at a rate high enough to transform some of the austenite to martensite. Dual-phase steel can be produced in the as-rolled condition by carefully controlled continuous cooling after rolling [15] or by quenching after rolling in the intercritical region [9]. These methods have the advantage of eliminating a heat treatment step for obvious cost savings. The composition of dual-phase steel usually consists of 0.06-1.5% C, 0.3-1.5% Mn, 0.3-2% Si, and may also contain small amounts of vanadium, niobium, chromium or molybdenum. This low alloy content makes dual-phase steel simple and inexpensive. Despite the lean nominal alloy composition, martensite can be formed with moderate cooling rates. This is possible because of the segregation of carbon and alloying elements to the austenite during two phase annealing [14,16-18] which can substantially increase the hardenability of the austenite.

The mechanical properties typical of this composite microstructure include low yield strength, continuous yielding, high initial work hardening rate, high tensile strength, good ductility, and good formability. Fig. 1 contains typical stress strain curves of dual-phase steel [19] and a stress strain curve of a ferrite-pearlite steel included for comparison. The low yield strength is the result of deformation beginning in the soft, clean ferrite matrix. The lattice shear and volume expansion of the austenite to martensite transformation causes a distortion

between the product martensite and the matrix [20]. This distortion generates residual stresses and introduces a high density of mobile dislocations into the ferrite around the martensite particles resulting in a lower yield strength than ferrite–pearlite steels. The mobile dislocations and the residual stresses allow deformation to start immediately at many different locations resulting in continuous yielding.

The early yielding is followed by a high initial work hardening rate. High work hardening is typical of materials consisting of a hard dispersion in a soft matrix and is enhanced by the elimination of the residual stresses mentioned above. This initial work hardening stage is followed by two stages of lower work hardening after the back stresses are eliminated and as dislocation cells form.

The rapid work hardening provides a high tensile strength despite the low yield strength and suppresses the onset of necking in uniaxial tension tests to yield high uniform elongation values. More importantly it suppresses the onset of plastic instability in multiaxial metal forming operations to yield improved formability [21].

Since dual–phase steel is a composite, its mechanical properties should be influenced by the mechanical properties and volume fractions of its components as predicted by composite strengthening theory. This is especially true for the yield and tensile strengths which have been shown to have direct linear relationships with the volume fraction of martensite [22, 23]. Deviations from this trend can be attributed to changes in the

strength of the martensite because of changes in the carbon content at different annealing temperatures [24], or to changes in the strength of the ferrite because of precipitation strengthening [25-27].

As the understanding of the fundamental physical and mechanical metallurgy of dual-phase steel progressed, the emphasis of research on dual-phase steel shifted toward optimizing alloying and processing to obtain better properties at lower cost. However, in our alloy design program at Berkeley, an attempt has been made to draw upon the many advantages of this composite microstructure for use in applications other than for cold formable sheet. One example was the design of a dual-phase steel for low temperature structural applications [9]. The design concept was to combine the high strength and good ductility of dual-phase steel with very fine grain size obtained through controlled rolling. The result was an as-rolled dual-phase steel with an excellent combination of strength and low temperature impact toughness.

The application for dual-phase steel being considered in this research is that of high strength wire. Designing a dual-phase steel for cold drawing into wire is quite a large departure from the norm since most of the present applications for dual-phase steel are in sheet products. Dual-phase steel was selected in this case because of its pronounced strain hardening rate and superior formability. The rapid strain hardening helps to increase the strength further above the nominal 50 ksi (345 MPa) yield strength with less cold reduction. The superior formabil-

ity increases the amount of drawing strain that can be applied to the steel, increasing the maximum strength attainable. The superior formability also makes the wire drawing process itself simpler and more reliable. The wide range of mechanical properties possible with dual-phase steel allows one to tailor the steel to the specific application and wire drawing parameters encountered. These advantages are in addition to the previously mentioned simplicity and low cost of the composition and processing.

The present process for producing high strength wire begins by patenting a steel of 0.4% carbon or higher. Patenting is a continuous heat treating process used for wire production [28]. It consists of heating the as-received hot rolled rod above the upper critical temperature for a short period of time followed by rapid cooling to a set temperature where the austenite is transformed to the desired fine pearlitic structure. Air patenting involves heating the rod by pulling it through a open furnace followed by open air cooling. Faster and more accurate heating and cooling can be achieved by using molten lead or direct resistance heating followed by quenching in a lower temperature molten lead or molten alloy bath. The patenting process is followed by heavy drafting to high strengths in the desired finish diameter. If very high strength and/or small diameters are desired, the wire must be patented more than once before the desired size and properties are reached.

The cold deformation of iron begins with formation of relatively straight dislocation lines [29]. Dislocation interaction

begins at about 1% strain, and after about 3.5% strain, the dislocations begin to cluster and form a cell structure. By 9% strain, these cells are well defined and the dislocation density in the cell interiors is low. As the strain increases, the cells begin to align themselves. At higher strains, such as those encountered in wire drawing or cold rolling, the cells begin to elongate in the working direction and decrease in width. At this point, the flow stress is linear with $d^{-1/2}$ where d is the cell width [30,31].

As in most BCC materials, pure iron and pearlite develop a [110] texture during wire drawing [32,33]. A BCC crystal in a [110] orientation can only elongate by slip in the $[1\bar{1}1]$ and [111] directions, resulting in a net contraction along [001] [32,33]. There is no net change along $[1\bar{1}0]$. This plane strain deformation of the cells and grains give them an eliptical rather than circular transverse section. As a result, they must curl around each other to maintain compatibility. This gives BCC wires a wavy appearance in transverse sections [32-34]. This extra curling strain is thought to be a source of increased strain hardening after 70% reduction.

The strain hardening rate of pearlite is higher than that of a single phase BCC material such as pure iron since the cementite fragments stabilize the cell walls against dynamic recovery and the pearlite spacing establishes a smaller initial cell size [31]. At higher strains, the cell size is proportional to the wire diameter. Thus, the flow stress is also linear with the wire diameter raised to the one half power, resulting in the flow

stress being proportional to exp(ε/4) [30], where ε is the true strain.

Fine pearlite is more desirable than coarse pearlite. It is not only stronger, but it strain hardens faster [30], can be drawn further [30], and deforms in a more ductile manner [35,36]. Continued drafting of pearlitic wire leads to void formation. Void formation in pearlitic wire occurs by fragmentation or decohesion of the cementite [36].

In general, decohesion at the interface of a hard inclusion in a ductile matrix must satisfy two criteria, an elastic energy criterion and an interfacial stress criterion [37]. The elastic energy criterion is that the elastic energy stored in the plastically non-deformable inclusion which is released during decohesion must be greater than or equal to the energy of the newly formed surfaces. This is why the particle/matrix interfacial energy has such a strong influence on the nucleation rate of voids [38]. This criterion is more easily satisfied for large particles than for small particles [37]. The second criterion is that the stress (tensile) at the particle/matrix interface must exceed the tensile strength of that interface before the stored elastic energy can be released to form the two new surfaces.

Studies on the formation of voids in the necked region of a tensile specimen of a ferrite-spherodized carbide steel [39] and a ferrite-martensite steel [40] have shown that decohesion tends to occur at the particle/matrix interface, more specifically, at one pole of the particle, between closely spaced particles, at particles that are of greater than average size, at elongated

particles, and at particles lying at ferrite-ferrite grain boundaries. These observations can be explained by considering the elastic energy of the particles, the energy of the particle/matrix interface and the tensile stress on the interface. One exception, however, is the observation that voids tend to form at elongated particles. The criteria for void formation presented earlier was derived for equiaxed particles and do not necessarily apply to elongated particles. Another assumption was that the particles do not plastically deform at all which does not apply to some martensite particles. Fiber composite theory states that an elongated particle has a better load transfer with the matrix [41] which would tend to reduce void formation. The occurrence of voids at larger than average particles may also be a consequence of greater interaction with other particles rather than just their size [37].

In his study of a 1.5% Mn dual-phase steel, Speich [24] found that void formation began either by decohesion or cracking of the martensite second phase. He cited McClintock [42] as saying that the reduction in area is dependent in a complex manner on the nucleation and growth of voids, and used this to reason that the reduction in area can be used as a measure of the void formation tendency of different microstructures, i.e., of different martensite carbon contents and volume fractions. He derived an empirical relation showing that reduction in area is inversely proportional to the carbon content of the martensite times the square root of the volume fraction of martensite. Thus, carbon content has a much greater influence than volume

fraction on reduction in area, and therefore, a greater influence on void formation.

The first step in this research was to learn more about the high strain deformation behavior of dual-phase steels during wire drawing. Except for a fundamental deformation study by Korzekwa et al. [43], very little is known about wire drawing of dual-phase steel. A study on the deformation of dual-phase steel is also beneficial to the numerous existing applications of dual-phase steel that require cold forming during processing. Dual-phase steel is ideal for a fundamental study on the deformation of a two phase system since a wide range of structures can be produced from a single alloy. The martensite particle size, shape, strength, volume fraction, and distribution within the ferrite matrix can all be changed to a large degree by changing the heat treatment path and the two phase annealing temperature.

Wire drawing is an ideal process for a fundamental study on deformation since it allows very large plastic strains to be attained. This is because although the work of the deformation is applied through tension of the wire at the exit of the die, plastic flow is caused by indirect compression from the die surface [41]. Also, the axisymetric geometry of the process results in more uniform deformation than other large strain deformation processes such as flat rolling, thus simplifying analysis and improving properties.

The Fe/Si/C dual-phase steel was chosen for this study because it was previously shown to have excellent mechanical properties [13]. The system is also well characterized in terms

of both microstructure and mechanical properties [13,14,18,25,44, 45]. In addition, it was shown that a wide range of morphologies and mechanical properties could be produced from a single alloy through appropriate thermal processing [14,45], thus allowing for a more thorough and consistent investigation with fewer changes in alloy composition. From an economic point of view, the alloy is simple and inexpensive. The silicon provides the added benefit of solid solution hardening [46]. This makes it possible to obtain higher strength levels in the drawn wires with less cold work without sacrificing ductility [47].

The deformation behavior was studied in terms of the difference in strain between the hard and soft phases, the formation of voids that result from this difference, the structure of highly deformed ferrite and martensite, and the effect of the ferrite and martensite morphology on the wire drawing behavior of these steels. Correlations were made between the initial structure and properties of the different dual-phase steels, and the structure and properties of the drawn wire.

The second step and ultimate goal was to use the information gathered during the fundamental study of the deformation of dual-phase steel during wire drawing to propose a design of a dual-phase steel of appropriate microstructure and properties for cold drawing into high strength wire. A successful design must have a simple alloy composition and must attain the desired properties without intermediate heat treatments or anneals.

2. EXPERIMENTAL PROCEDURE

2.1 Material Preparation

The alloy codes and the chemical compositions of the alloys used in this investigation are shown in Table 1. The 2% silicon alloys SV and S were provided by Sandia National Laboratories, Albuquerque, N.M. They were vacuum induction melted in 300 lb (130 kg) ingots and vacuum arc remelted. They were homogenized at 1100 C for 16 hours and hot worked to 0.525 inch (13 mm) thick plates. Rectangular bars 0.5 inch (13 mm) wide were cut from these plates and hot rolled to rods approximately 0.290 inch (7 mm) in diameter. The 1.5% manganese alloy was provided by Nippon Kokan K. K. It was vacuum melted and cast in a 110 lb (50 kg) ingot. After soaking at 1200 C for two hours and hot rolling, the billet was cut into smaller pieces and hot open die forged into bars 0.65 inch (16.5 mm)in diameter and 6-1/2 feet (2 m) long. These bars were then hot rolled in the same manner to 0.290 inch (7 mm) rods.

2.2 Heat Treatment

Oversized blanks 0.250 inch (6.4 mm) in diameter were machined for drawing into wire (4 inches in length) and tensile test specimens (2-3/4 inches long). These were then heat treated in a vertical tube furnace under flowing argon atmosphere according to the schedules shown in Fig. 2. Austenitizing for the double heat treatment was one hour at 1150 C for all cases. The two phase annealing was done for ten minutes at 850 C to 1000 C

for the 2% Si steels and at 757 C for the 1.5% Mn steel. Both heat treatments were completed with a quench into agitated iced brine. Minor variations to the above treatments were used occasionally and are described in the text.

2.3 Wire Drawing

The 4 inches (102 mm) long heat treated blanks were machined to a diameter of 0.200 inch (5 mm). They were then pointed by swaging and drawn through 6°–8° semi-die angle conical carbide and diamond dies lubricated with Dupont Vydax Freon-Teflon dispersion. The usual drawing speed was 1.2 inch/sec (31 mm/sec) resulting in a strain rate of 3/sec in the larger sizes to 33/sec in the smaller sizes. The usual reduction in area per pass decreases from 35% in the early stages to 20% in the later stages.

2.4 Metallography

2.4.1 Optical Metallography

Specimens for optical metallography were cut from heat treated rods the same diameter as the tensile specimen blanks and as the rods used for wire drawing to ensure similar heating and cooling rates. After mounting in either a self curing resin or a clear thermoplastic compression molding material, the specimens were rough ground on a flood cooled 240 grit belt sander, then hand ground on wet silicon carbide paper from 240 grit to 600 grit. The final polishing was done with 6; then 1; diamond paste on a nylon cloth covered polishing wheel. After the microstructural features were revealed by etching in a 2% Nital solution

for 30-60 seconds, the microstructures were observed and recorded with a Zeiss Ultraphot II metallograph using Polaroid film. Martensite volume fractions were determined by the line intercept method [48] using several micrographs taken at 1000 times magnification.

2.4.2 Scanning Electron Microscopy (SEM)

Specimens for scanning electron microscopy were prepared in the same manner as those for optical metallography. They were observed either in an AMR-1000 scanning electron microscope operated at 20 kV or an ISI DS-130 scanning electron microscope operated at 25 kV. X-ray microanalysis was performed on the AMR-1000 SEM which was equipped with a Kevex energy dispersive spectrometer (EDS) system.

2.4.3 Transmission Electron Microscopy (TEM)

Thin foils for transmission electron microscopy of the as-heat treated steels were obtained from the same heat treated rods used for the preparation of specimens for optical metallography. Slices approximately 12 mils thick were cut with an Isomet low speed saw using a diamond wafering blade. The slices were then chemically thinned to 2 mils at room temperature in a solution of 96 ml of 30% H_2O_2 and 4 ml of 48% HF. After the 3 mm dics were punched from the slices, they were polished to electron transparency in a twin jet electropolisher using a solution of 75 grams CrO_3, 400 ml CH_3COOH and 21 ml of distilled water. Polishing potentials of 35-50 volts were used. The thin foils were then

examined with a Philips EM301 transmission electron microscope at an accelerating voltage of 100 kV.

Longitudinal sections of the drawn wires were made by hand grinding two sides of the wire to make a thin strip 2 mils (0.05 mm) thick and as wide as the original wire diameter. This strip was then polished by the window technique in a solution of 1 pound (0.5 kg) anhydrous sodium chromate and 1 gallon (3.8 l) glacial acetic acid using a polishing potential of 25-35 volts. Smaller wires were thinned without masking the edges of the strip.

Transverse sections of the drawn wires were made by nickel plating the wire to a total diameter of 3 mm and slicing off 0.012 inch (0.3 mm) thick discs with the low speed saw. These discs were then hand ground on wet silicon carbide paper to a thickness of 2 mils (0.05 mm) and jet polished as above.

2.5 Mechanical Testing

2.5.1 Tensile Testing

Testing of the steels in the as-heat treated condition was conducted on subsize cylindrical specimens machined from the 2-3/4 inch long blanks according to the specification shown in Fig. 3. This was done at room temperature on an Instron machine at a strain rate of 0.04/min. Total elongations were determined by measuring the distance between two marks approximately 0.5 inch (13 mm) apart before and after testing with an optical microscope equipped with a vernier translating stage having a precision of 0.01 mm (0.4 mil). The reduction in area was calcu-

lated from measurements made on this same microscope. The other tensile properties were determined from the load-displacement curve recorded by the testing machine. The yield strengths were determined by the 0.2% offset method.

The drawn wires were tested on the Instron testing machine in 3-1/2 inch (89 mm) lengths with 1 inch (25.4 mm) gauge lengths. The strain rates were 0.005-0.02/minute. The wires larger than 0.075 inch (1.9 mm) in diameter were tested in self tightening wedge grips. In this case the gauge diameter was reduced by 10% to prevent failure in the grips. Smaller diameters were tested in screw tightened grips. The jaws were lined with aluminum strips to prevent failure in the grips. The ends of the wires were roughened with coarse emery paper to prevent slipping.

2.5.2 Torsion Testing

Torsion testing was done on 6 inch (152 mm) long specimens with 4 inch (102 mm) gauge lengths. The ends of the specimens were gripped in the chucks of a lathe and the lathe was turned by hand until failure of the wire. The number of times marks on each end of the gauge passed each other was recorded. This ensured that that twisting in the grips or outside the gauge was not recorded.

2.5.3 Microhardness Testing

Wire sprecimens for Vickers microhardness testing were mounted in a self curing resin and polished as in preparation for

optical metallography. They were then tested in the axial direction with a Leitz Miniload microhardness tester using a 1 kg load. The reported figures are the average of at least ten measurements.

3. RESULTS

3.1 Structure

3.1.1 Initial Structure

The initial as-heat treated structures of the dual-phase steels are shown in Fig. 4. In these optical micrographs, the dark etching phase is martensite and the light etching phase is ferrite. The volume fraction of martensite for each structure is given in Table 2. As expected from the tie-line construction for the corresponding phase diagram, the volume fraction of martensite increases with annealing temperature as seen by comparing Figs. 4a-c. The carbon content of the martensite was estimated by dividing the bulk carbon content of the alloy by the volume fraction of martensite. This is a rough estimate since it neglects the carbon content in the ferrite, but it gives a rough idea of the strength/hardness of the martensite. The results are included in Table 2.

The double heat treated silicon containing alloys have the characteristic acicular martensite particles with some grain boundary allotriomorphs. There is no significant difference between the two silicon containing alloys except for a decrease in the volume fraction of martensite and the possible precipitation of vanadium carbide with the addition of vanadium. The change in the martensite volume fraction may be attributed to the fact that vanadium constricts the austenite phase field [46] resulting in a lower austenite volume fraction (and thus a lower martensite volume fraction) at a given annealing temperature.

The single heat treated specimen has a fine, uniform dispersion of equiaxed martensite particles. The martensite volume fraction is essentially the same as in its double heat treated counterpart.

The double heat treated alloy M also has acicular martensite particles, however, the number of grain boundary allotriomorphs and idiomorphs has increased to the point that the martensite is continuous at the prior austenite grain boundaries. The microstructure also contains several large intragranular idiomorphs.

The second phase of the silicon containing alloys was found to be predominantly lath martensite as shown in Fig. 5. Thin films of retained austenite between the laths were found by selected area diffraction and dark field analysis. As mentioned earlier, this is the preferred substructure for a martensitic steel, as well as for a ferritic-martensitic dual-phase steel. Microdiffraction analysis of the double heat treated specimens showed that the martensite particles generally have the same crystallographic orientation as the surrounding ferrite matrix (Fig. 6). This is generally not true for the martensite in the single heat treated specimen.

3.1.2 Drawn Structure

Fig. 7 shows the drawn structure at a true strain of 3.6 or 97.3% reduction in area. In these scanning electron micrographs, the brighter phase is the martensite. Both the ferrite and the martensite in the dual-phase steels deform, but to greatly

varying degrees. This difference in strain results in void formation at the ferrite/martensite interface. Martensite particle cracking was not observed at this strain. A martensitic steel quenched from the austenite phase field, SV SING 1150 (Fig. 7e), was included for comparison. This single phase material deforms much more homogeneously.

The results of void area density measurements made on polished and etched longitudinal sections of drawn wire are presented in Table 3 with the SV DBL 850 specimen having the highest density and the martensitic specimen having the lowest. The void density was measured in micrographs taken at 505 X and averaged from an area of approximately 0.1 mm^2. Only voids 0.5 ;m in diameter or larger were counted. As shown in Fig. 8, there is a direct relationship between the void density and the estimated carbon content of the martensite. Most of the voids occur at the interface between the martensite particles and the ferrite matrix although some small voids were caused by inclusions in the steel.

The voids that form at the ferrite/martensite interface during wire drawing can eventually coalesce to cause failure during subsequent tensile loading or at the die exit during a drawing step as shown in Fig. 9. Martensite particles can be found at the bottom of the fracture dimples in much the same way as inclusions.

Fig. 10 shows the progression of the dual-phase structure as the strain was increased from 0 to 3. This series of specimens was used to determine the ratio of the strain in the martensite to

the total strain of the wire. The results of this experiment are shown in Table 4. The initial microstructure was produced by a double heat treatment modified by cold working the martensite prior to two phase annealing. This produces a more equiaxed structure than the conventional double heat treatment, thus simplifying the strain measurements. The particles were found to fall into three basic groups: 1) small, nearly equiaxed particles approximately 2 μm in size, 2) acicular particles 2–3 μm wide and 5–10 μm long and 3) large, nearly equiaxed particles up to 30 μm in diameter. There were also some irregularly shaped particles apparently made up of smaller particles which had impinged upon each other during two phase annealing. The particles in groups 1 and 3 were found to have an aspect ratio of approximately 1.6. This value is a low estimate since particles with their major axis not lying in the section plane appear to have a smaller aspect ratio, thus reducing their contribution to the average aspect ratio. The extreme case is a particle whose major axis is perpendicular to the section plane, which in this case would appear to have an aspect ratio very close to one in two dimensions.

After drawing to a true strain of 1, all of the particles were aligned with the wire axis. Some voids were beginning to form at the ferrite/martensite interfaces. Many of the smaller particles were still equiaxed, indicating that they had not begun to deform at this point. Those small particles that appear to have elongated along the wire axis were initially acicular and have simply rotated to align themselves along the wire axis

without deforming. The large particles had an aspect ratio of 3.5 which becomes 2.2 when corrected for the initial aspect ratio of these particles. The strain corresponding to this aspect ratio is 0.52 which gives a martensite strain ratio of 0.52 at a wire strain of 1. This says that the martensite deforms only half as much as the bulk wire. The smaller equiaxed particles began deforming at a strain of 3 and had a strain ratio of 0.11 at this point. The small acicular particles are closer to ideal fibers and presumably began to deform earlier since they are loaded more efficiently. However, it is difficult to separate the initial aspect ratio from strain and the point at which the small acicular particles began to deform could not be determined. The deformation at a strain of 3 was too severe to determine the aspect ratio of the large particles.

Fig. 10b shows two examples of non-metallic inclusions found in alloy S. The inclusion marked A has caused a void to form in the martensite phase, whereas the inclusion marked B did not cause a void to form in the ferrite matrix in which it lies. These vacuum melted experimental steels are generally clean and as mentioned earlier, the voids that they do cause are much smaller than those associated with the martensite particles. However, they are more important in a steel with a low void density such as the martensitic specimen. An EDS analysis of these inclusions showed that they are titanium rich. Since there was no titanium in the nominal composition of these steels, the inclusions must be contamination from a previous heat.

When the drawn wires are observed in the transmission elec-

tron microscope (Fig. 11), one can see the fine cell structure that develops in the ferrite. An example of a non-deforming martensite particle is shown in Fig. 12. The highly deformed ferrite flows around the martensite and develops a fine cell structure. Although the martensite is heavily dislocated from the martensitic transformation, it is not deforming and shows no sign of cell formation at this point. Fig. 13 is a transverse section of another non-deforming martensite particle in a highly deformed ferrite matrix.

Fig. 14 shows the strong [110] wire texture that developed in this BCC wire. The wavy structure that results from this texture can be seen at low strains in the optical microscope (Fig. 15) or at higher strains in the transmission electron microscope (Fig. 16).

3.2 Properties

3.2.1 Initial Properties

The tensile properties of the as-heat treated steels are summarized in Table 5. A look at the yield and tensile strengths for alloy SV shows that they follow the law of mixtures for dual-phase steels, increasing for higher volume fractions of martensite. The vanadium addition did not cause a decrease in strength for higher volume fractions as observed in some steels containing niobium [25-27]. The ductility generally increased as the strength decreased except in the case of the double heat treated manganese containing alloy which had poorer properties overall than the rest of the specimens.

3.2.2 Drawing Properties

Table 6 gives the drawability rankings for the different specimens based on the maximum strain before repeated breakage occurred at the die exit. A comparison of the three double heat treated alloy SV specimens shows that the drawing limit decreased for higher volume fractions of martensite. The important role of the other morphological factors is shown by the high drawing limit of the martensitic specimen and by the low drawability of the manganese steel and the single heat treated steel.

3.3.2 As-Drawn Properties

The increase in Vickers hardness as a function of true drawing strain is plotted in Fig. 17 for different volume fractions of martensite in the SV alloy given the double heat treatment (including the single heat treated martensitic specimen). The hardness in the as-heat treated condition increased as the volume fraction of martensite increased, consistent with the law of mixtures. The hardness difference between the specimens generally remained the same throughout the range of the plot. This shows that the hardness increase as a function of strain is almost the same even though the martensite volume fractions cover a wide range.

Table 7 lists the ultimate tensile strengths of the drawn wires at a strain of 3.6. The Vickers hardness numbers are also listed for comparison. The results indicate that there is not as much difference in the strengths as suggested by the wide range in hardness values. As will be discussed later in section 4.3,

the strength values do not even follow the same trend as the hardness values. The yield strengths were essentially the same as the tensile strengths and there was no measurable reduction in area in this un-stress relieved condition.

3.3 Effect of Processing

3.3.1 Quench Rate After Two Phase Annealing

A very good quench after two phase annealing is necessary to produce the desirable duplex ferrite/lath martensite microstructure. Slow or delayed quenching can cause significant shrinkage of the austenite pool prior to its transformation to martensite. One possible consequence of this is shown in Fig. 18. This transmission electron micrograph of the ferrite/martensite interface shows a region of microtwinned martensite at the edge of a predominantly lath martensite particle. The presence of the microtwinned substructure indicates that this martensite has a higher carbon content than the rest of the particle and thus formed from austenite enriched in carbon as the austenite pool shrank during the poor quench. The ferrite region adjacent to the interface is presumably the new ferrite or epitaxial ferrite that formed behind the moving γ/α interface [49,50]. The example shown in Fig. 19 is not as common, but is much more severe. In this transmission electron micrograph, some of the austenite has transformed to ferrite and carbide during a poor quench. The effect of quench rates will be discussed further in section 4.5.2.

3.3.2 Drawing Schedule

The four most important wire drawing parameters are the drawing schedule, i.e. the amount of reduction in area per pass, the drawing speed, the die cone angle, and the coefficient of friction. The drawing schedule could be changed through by-passing dies to increase the reduction in area per pass and the drawing speed could be varied in the early stages over a small range. There was little or no control of the die cone angle nor the coefficient of friction. Drawing was always done in the same direction since pass reversal results in poorer properties and higher residual stresses [51].

Three different schedules were used: one with small reductions per pass (3-9%), one with large reductions (37%), and one that gradually decreased from 32% to 21% reduction per pass. In all cases, the the steel was alloy SV double heat treated to 36% martensite with an initial diameter of 0.22 inch (5.5 mm).

The maximum drawing strain obtained with the small reductions per pass was 1.2. The light passes resulted in central bursting as shown in the composite Fig. 20. This wire was drawn on an Instron machine and the load fluctuations characteristic of central bursting were detected by the load cell at a strain of only 0.9. The bursts and the load fluctuations grew during subsequent passes until the cracks reached critical size at a strain of 1.2 and caused failure at the die exit.

Drawing with larger reductions of 37% eliminated the central burst problem and resulted in a maximum drawing strain of 3.6. In this case, the larger reductions resulted in a larger

drawing load. This put greater stress on the drawn wire and caused premature failure through increased internal damage.

The graduated schedule had a moderately high reduction of 32% per pass in the early stages where central bursting is a greater problem and gradually decreased to 21% per pass to reduce the drawing load while remaining in a region which is apparently safe from central bursting for this material. This resulted in a maximum drawing strain of 6.3 or a total reduction in area of 99.8%.

3.3.3 Drawing Speed

A comparison was made between drawing at 1.2 inches/minute (31 mm/sec) and 4 inches/minute (103 mm/sec). In this study, the steel was the SV alloy double heat treated to 18% martensite. The wire was drawn in four passess of 32-37% reduction per pass from 0.220 inch (5.5 mm) to 0.0907 inch (2.3 mm) in diameter. As reported in Table 8, the high drawing speed caused a general deterioration of the properties. Tests at lower speeds done on the Instron machine showed that the drawing loads also increased significantly as the drawing speed was increased.

3.3.4 Stress Relief

The cold worked wires have a large amount of internal stress both on a microscopic scale from the large amount of deformation, and on a macroscopic scale from the inhomogeneities in the wire drawing process. This residual stress takes the form of longitudinal compression on the surface and longitudinal tension in the

interior as well as radial and tangential stresses [51]. This is a major factor in the brittle tensile behavior of the as-drawn wires. A double heat treated SV alloy specimen was drawn from a diameter of 0.220 inch (5.5 mm) to 0.037 inch (0.93 mm) in eight passes and stress relieved at 400 C for 3 minutes which is similar to industrial practice for patent wire. The specimens were tested in tension and in torsion in the stress relieved and un-stress relieved condition. As shown in Table 9, the stress relief provided significant gains in torsional ductility and reduction in area without much loss in tensile strength. A photograph of the specimens after the torsion test (Fig. 21) shows the effect on the deformation behavior with the un-stress relieved specimen splitting into fibers (Fig. 21a) rather than shearing uniformly as in the stress relieved case, (Fig. 21b). As shown in Fig. 22, the fracture surface of the stress relieved specimen tested in torsion has a ductile dimple appearance.

4. DISCUSSION

4.1 Void Formation

There is a tendency for the harder, stronger phase of a composite to deform less than the softer phase. The results of section 3.1.2 show that the large martensite particles deformed approximately half as much as the bulk wire (true strain) and smaller particles deformed one tenth as much. This is a large difference in strain and that difference which could not be accommodated by the ferrite resulted in the formation of voids. The area density of the resulting voids varied greatly among the different structures studied.

As shown in Table 3, the void density was highest for the SV alloy annealed at 850 C and decreased with increasing annealing temperature. This is contrary to the fact that the SV DBL 850 specimen has the lowest volume fraction of martensite and strength, and has the highest ductility and drawing limit of the three double heat treated SV dual-phase steels. However, as discussed previously, void formation is more strongly dependent on the carbon content of the martensite than on its volume fraction. Thus, the decrease in the void formation tendency at a lower volume fraction resulting from a lower annealing temperature does not compensate for the increase in void formation tendency due to the higher carbon content. This applies to cases such as the present in which the bulk carbon content is held constant and volume fraction and carbon content of martensite are essentially inversely related. The higher carbon martensite has

a higher yield strenth and is less plastic than the lower carbon martensite and thus has more stored elastic energy to satisfy the energy criteria for void formation. Speich attributed the increase in void formation at higher volume fractions to the decrease in the interparticle spacing, i.e., more nucleation sites. However, in this study, the higher volume fractions were derived from larger martensite particles and the number of martensite particles may have even been lower due to particle impingement and coalescence. This reduced the effect of volume fraction even further.

The other extreme is the martensitic specimen. In this case, the microstructure was homogeneous on a macroscopic scale. The only inhomogeneities on a microscopic scale were the interlath retained austenite films which are ductile and coherent with the martensite. Thus, the void density was very low with most of the voids resulting from non-metallic inclusions.

There are several reasons why the void density was higher in the single heat treated specimen than in its double heat treated counterpart. The volume fraction and hardness of the martensite is essentially the same since they are the same alloy annealed at the same temperature. The differences in the microstructures are in the shape of the martensite particles, their interface with the ferrite matrix and their location with respect to ferrite grain boundaries. The martensite particles in the double heat treated steel are acicular, whereas those in the single heat treated are roughly equiaxed. The acicular shape gives them better fiber loading, thus lowering the void density. In addi-

tion, the martensite is usually close to the same orientation as the ferrite and does not lie on ferrite-ferrite grain boundaries. These low angle boundaries tend to have lower interfacial energy [52]. As discussed earlier, this decreased the void formation tendency. The structure of the double heat treated steel will be discussed in more detail in section 4.5.

4.2 Drawing Limit

The drawing limit of dual-phase steel is very important since the a large part of the strength of the wire results from the cold drawing. A comparison of Tables 3 and 6 shows that there is no general correlation of the drawing limit with the void density. The only trend exists for the three double heat treated alloy SV specimens. Among these specimens, there is a direct relation between the void density and drawing limit. Unfortunately, this means that the specimen with the highest drawing limit, SV DBL 850, has the most voids as mentioned in the previous section. This may be due to the fact that the volume fraction of the ductile ferrite matrix is highest in this case. Voids that form under uniaxial stress conditions will tend to elongate only in the tensile direction without coalescing and without any detrimental effect on the strength [53]. Thus, the ferrite phase can continue to deform without further fracture. Voids that form under triaxial stress conditions such as those found in the neck of a tensile test specimen will tend to grow also in the transverse direction and eventually coalesce, resulting in failure of the material. The conditions in the die

during wire drawing are not exactly uniaxial, but the ferrite phase still fractures in a ductile manner on a microscopic scale even at the drawing limit of the wire (Fig. 9). In the higher volume fraction specimens, there is less ferrite and the voids cause the wire to fail as soon as the ductility of the martensite is exhausted.

The drawability is not a simple function of the ductility of the wire. Each draft is a test of the breaking strength of the wire at the exit of the die against the drawing load (mainly the resistance of the wire to deformation). The ferrite in the low martensite volume fraction specimen must bear the load of deforming the composite of ferrite + voids + small martensite particles, whereas the specimens with the higher volume fraction are weakened by the voids and must bear the load of deforming a harder material with much larger martensite particles.

The difference between the drawing limits of the single and the double heat treated alloy SV specimens cannot be attributed solely to the difference in the void density at a strain of 3.6. However, the same factors that caused the higher void density in the single heat treated specimen, i.e, high angle interfaces and matrix grain boundaries, allowed for increased void growth. Also, as shown in Table 7, the hardness of the single heat treated specimen was higher than that of the double heat treated specimen at this point. Thus, the same case of a wire with a lower tensile strength pulling a wire that is harder to deform through the die applies.

The case of the manganese steel is a little different since

it was double heat treated. However, as mentioned in section 3.1.1, the major difference between the double heat treated silicon and manganese containing specimens in the as-heat treated condition was the presence of the large, interconnected grain boundary allotriomorphs and idiomorphs in the latter. The first factor is that these martensite particles are preferential void nucleation sites since they are at the prior austenite grain boundaries. Also, their close proximity to each other increases their void formation tendency further [37,39,40]. Once voids nucleated at these sites, they could easily coalesce since they form a continuous network with no ductile ferrite to bear any load.

4.3 Mechanical Properties of Wire

The hardness of a material will generally increase as it is drawn to higher strains. However, as shown in Fig. 17, the hardness of the wire drawn from the SV alloy double heat treated at 850 C and 950 C decreased after a maximum at a true strain of 5.4. This decrease in hardness may have been due in part to dynamic recovery. As discussed previously, the cementite particles are responsible for retarding dynamic recovery in the ferrite of drawn pearlite. The lower volume fraction of martensite in these specimens results in a higher volume fraction of ferrite with a larger mean free path between martensite particles. Internal damage in the form of voids may have also been a factor in the decrease in hardness. The two specimens that had this behavior also had the highest void density (Table 3) of those plot-

ted in Fig. 17. The mechanical fibering and loss of ductility in some of the wires caused a few of the specimens to fracture during indentation with the 1 kg load. Although these fractures were easily detected allowing the tests to be rejected, more subtle microcracking could occur to give low hardness values.

The effect of overdrafting can also be seen in the tensile strengths of the drawn wires (Table 7). Among the double heat treated SV alloy specimens, SV DBL 850, SV DBL 950 and SV DBL 1000, the SV DBL 1000 had the lowest strength even though it had the highest hardness. This is mainly because of the brittle behavior of the wires in this un-stress relieved condition. The hardness of the SV DBL 1000 specimen could not be fully utilized during the tensile test since brittle fracture occurred before yielding. As mentioned in the previous section, the ferrite in the lower martensite volume fraction specimens was still ductile on a microscopic scale.

An important processing variable discussed in section 3.3.3 is the drawing speed. There are three main effects of increasing the drawing speed. The first is the increase in the strain rate. The second is a possible break down of the lubrication and the third is the reduction in the time for heat dissipation which leads to higher wire and die temperatures. The result of the first two effects was the observed increase in the drawing load. This lead to increased internal damage to the wire since the drawn wire at the exit of the die had to bear the heavier drawing load. This can lead to decreased strength and ductility as discussed previously. The increased heating of the wire has a

greater effect on the temperature of the wire as it exits the die rather than on the wire as it is being deformed. Thus it will not tend to decrease the drawing load. It will, however, increase the amount of dynamic recovery which will cause a further decrease in the strength of the wire.

4.4 Central Burst

When light pass reductions were taken, the wire failed after a very small total strain because of central bursting. The tendency for this metal working defect to occur increases as the pass reduction and the strain hardening of the material decrease, and as the die angle and coefficient of friction increase. The metal flow during wire drawing can be divided into three velocity fields. The velocity of the metal in the plastic zone gradually increases from that of the large inlet wire to that of the faster moving outlet wire. If the conditions conducive to central bursting exist, then the velocity fields take on the configuration shown in Fig. 23. The depth of deformation zone is too shallow and the center of the wire remains rigid. Since it is rigid, it cannot accomodate the incompatibility between the rigid inlet and the faster moving rigid outlet wire so it fractures, causing a burst to form. This relieves the incompatibility and allows sound metal flow to resume with uniform plastic deformation occurring between the two rigid zones. Eventually, the plastic zone narrows again to create another burst and the process repeats itself. The cyclic nature of central bursting manifests itself in the form of a fluctuating drawing load and

speed. The load is at a minimum and the speed is at a maximum when the burst is exiting the die. This fluctuation was detected several passes before the final failure of the wire occurred.

Once central burst failure was identified as the cause of premature failure during drawing with light reductions, it was necessary to determine amount of reduction necessary to avoid this problem. Avitzur presented empirical criteria for the critical reduction [54]. According to his diagram, a semi-die angle of 6° and a friction coefficient of 0.1 requires at least 37% reduction per pass to be safe from central bursting. This is a conservative value that guarantees that central bursting will not occur, but is not necessarily the minimum value needed, especially for ductile and high strain hardening materials.

The upper limit in the reduction per pass is the point where the drawing load exceeds the breaking strength of the wire at the exit of the die. This is given by Caddell [55] as:

$$r_{max} = 1 - e^{-\eta(n+1)}$$

where η is the efficiency of the drawing process taking into account friction and redundant work, and n is the strain hardening exponent. This value is usually in the range of 0.20 [21,24] to 0.35 [21] for dual-phase steel. Thus, a theoretical maximum reduction per pass is 74%. However, this value is greatly reduced by η in actual processes and applies only to the first pass since the value of n decreases with strain [24].

An analytical approach to the critical reduction per pass is

to determine the homogeneity of the deformation by calculating the deformation ratio Δ. This ratio is given by:

$$\Delta = H/L$$

where H and L are the characteristic height and length respectively of the deformation geometry. For wire drawing, this ratio is given by [56]:

$$\Delta_W = \alpha/r \left[1 + \sqrt{1-r} \right]^2$$

where $r = 1 - (d_1/d_0)^2$,

α is the semi-die angle in radians, d_0 is the diameter of the wire entering the die, and d_1 is the diameter of the wire exiting the die. Homogenous deformation is defined by a ratio of 1 or less and a ratio of 2 or greater produces very inhomogenous deformation [57]. According to this criterion, a semi-die angle of 6° requires 34% reduction to give a Δ of 1.

Thus, a conservative empirical approach gives 37% reduction per pass as the minimum to avoid central burst and an analytical approach yields 34% reduction per pass. As mentioned in section 3.3.2, the conservative value of 37% was too high and an empirically derived schedule was eventually used.

4.5 Double Heat Treatment

As shown earlier, the double heat treated steels containing

silicon were far superior to the single heat treated dual phase steel. The purpose of this section is to discuss the reasons for their superiority and the critical processing factors for correctly obtaining this structure.

4.5.1 Structure

In addition to the shape of the martensite particles in the double heat treated steel, the crystallography of the structure is an important feature. As shown in Fig. 6, the martensite particles generally have the same crystallographic orientation as the surrounding ferrite matrix, (111) in this case. This memory effect [58] has been shown to be detrimental to fracture toughness [58] and impact toughness [59] in steels given a heat treatment similar to the double heat treatment used in this investigation. This was attributed to the continuity of the (100) cleavage planes across the ferrite/martensite interface.

The memory effect and its consequences can be explained with the aid of Fig. 24. These two optical micrographs follow the microstructural changes of alloy S during a double heat treatment cycle. Fig. 24a shows the martensitic structure after austenitizing at 1150 C for 1 hour followed by a rapid iced brine quench. A single martensite packet comprises most of the figure. The martensite laths within the same packet are generally aligned in the same direction and usually have close to the same crystallographic orientation [60]. Upon two phase annealing, the austenite nucleates and grows at the lath boundaries to form the structure shown in Fig. 24b taken from the same area as Fig. 24a.

Because of the necessary re-polishing and etching, there is a small change in the section plane and resulting slight changes in the location and shape of the packets. However, it is easy to see that the alignment of the laths is retained in the orientation of the acicular martensite particles.

The memory effect is that the austenite formed during two phase annealing has a strong tendency to transform back to the same variant of BCC as the original martensite [58] which by this point has recovered to form the ferrite matrix. The alignment of the martensite particles and the crystallographic orientation of both the martensite and the ferrite is the same within a prior packet. Thus, a cleavage crack would pass straight through a prior packet and change its direction only at prior packet boundaries or at prior austenite grain boundaries resulting in poor toughness [58].

Void formation, however should be more difficult at the low angle ferrite/martensite interface than at the high angle ferrite/martensite boundary found around a martensite particle in the single heat treated microstructure. This is because a low angle boundary is generally of lower energy than a high angle boundary [52] and as mentioned earlier, the interfacial energy has a very strong influence on void formation. Koo has shown that in some cases, this interface can be coherent, thus reducing the energy further [61].

The ferrite/martensite interface in the single heat treated specimen is generally of high angle at least part way around the martensite particles because the particles generally lie on fer-

rite grain boundaries or at grain junctions. Thus, the martensite particle can have a low angle interface with at most one of the ferrite grains and must have high angle boundaries with the rest.

In some cases, the 2% silicon steels have martensite particles lying on prior austenite grain boundaries. However, as discussed earlier, this problem is not as severe as in the manganese containing steel.

4.5.2 Processing

Once it was determined that the best duplex structure consists of acicular martensite particles in a ferrite matrix of the same orientation, it was of interest to determine how this structure can be produced and to determine the critical processing factors.

The double heat treatment is obviously necessary since the first heat treatment provides the regions of similar orientation and laths to produce the acicular structure. It has been shown that the amount and type of substitutional alloying element plays and important role in determining whether or not austenite pools (eventually martensite particles) form at prior austenite grain boundaries [13,62]. Koo [13] found that silicon was necessary to prevent this. However, as found in this investigation, this is not sufficient.

A specimen of large surface to volume ratio, such as a thin rod being prepared for wire drawing, will tend to have large amounts of martensite at the prior austenite grain boundaries

This is shown in Fig. 25a which is an optical micrograph of alloy SV heat treated in the form of a 0.125 inch (3.2 mm) diameter rod. The martensite particles are also coarser and less acicular than those in a 0.250 inch (6.4 mm) diameter specimen (e.g. Fig. 4b). The large surface to volume ratio increases both the heating rates and both cooling rates during the heat treatment cycle [63]. Thus, it was necessary to determine which of the four heating/cooling rates was affecting the morphology.

The specimen in Fig. 25b was heat treated in the form of a 0.5 inch (13 mm) cube having a surface to volume ratio approximately one third that of the 0.125 inch diameter rod, slowing down the heat transfer considerably. The heating rate to the austenitizing temperature of 1150 C has at most a slight effect on the prior austenite grain size. The cooling rate from the two phase annealing temperature affects the shape, size and volume fraction of the martensite particles through austenite pool shrinkage prior to transformation to martensite as described earlier in section 3.3.1. This can be seen by comparing the martensite particle shape in Fig. 25a and Fig. 25b. Slowing the cooling rate from two phase changes the martensite particle boundaries from generally convex to generally planar or concave. However, while the heating rate to austenite and cooling rate from two phase are important for other reasons, they do not affect the location of the austenite pools/martensite particles. This leaves the heating rate to the two phase annealing temperature and the cooling rate from the austenitizing temperature as the possible critical factors.

It is well established that the primary heterogeneous nucleation sites of austenite in a lath martensitic structure are the prior austenite grain boundaries and the lath boundaries [62,64]. In order that the heating rate to the annealing temperature can be a critical factor, the following must be true. First of all, the martensite lath boundaries must be stronger austenite nucleation sites than the prior austenite grain boundaries in these steels. This is not impossible since the retained austenite at the lath boundaries and the boundaries themselves provide a high solute level and structural imperfection respectively for heterogeneous nucleation. In this case, a slow heating rate would provide a small superheat and thus a smaller driving force for nucleation of austenite. This would allow nucleation only at the more favorable lath boundary sites. The slow heating would allow time for these austenite pools to grow and to consume the carbon in the matrix, thus preventing nucleation and growth of the grain boundary austenite pools. The effect of a high heating rate would be to increase the driving force for nucleation, thus allowing austenite nucleation and growth at both sites.

Unfortunately, this explanation is not supported by experimental observations. Fig. 26 shows the effect of the heating rate to the two phase annealing temperature. Both of the specimens were 0.125 inch (3.2 mm) diameter rods austenitized and quenched the same way, and quenched from the annealing temperature the same way. The specimen in Fig. 26a was heated at 140 C/sec in molten tin and the specimen in Fig. 26b was insulated by

a 2 inch (51 mm) diameter steel bar to give a heating rate of 0.38 C/sec. This is compared to a heating rate of approximately 12 C/sec for the specimen in Fig. 25a. The only significant difference in the microstructures is the finer size and lower volume fraction of the martensite particles in Fig. 26a because of the higher nucleation rate at the laths and the reduced growth at the lower annealing temperature (approximately 900 C compared to 950 C). Both micrographs show a large amount of grain boundary allotriomorphs indicating that the heating rate to the two phase region had no effect on this feature. This leaves the cooling rate from the austenite phase field as the critical factor in the formation of grain boundary allotriomorphs.

Fig. 27a shows the effect of the quench rate from the austenitizing temperature on the subsequent two phase morphology. This specimen was austenitized and quenched in the form of a 0.5 inch (13 mm) cube and cut into a 0.125 inch (3.2 mm) thick slice prior to two phase annealing and quenching. There are martensite particles on prior austenite grain boundaries, but the structure is very similar to that of the bulk specimen Fig. 25b except for the reduced pool shrinkage and the resulting higher volume fraction of martensite and convex interfaces. A similar structure can be obtained in a 0.125 inch (3.2 mm) diameter rod by oil quenching after austenitizing and rapid quenching after two phase annealing.

As suggested by Koo [64], this effect is most likely the result of silicon segregation to the prior austenite grain boundaries where the repulsive interaction between the silicon and

carbon atoms [65] would prevent the nucleation of austenite at these sites. However, he concluded that the silicon segregation occurred during solution treating which does not account for the observed influence of the cooling rate. Another possible explanation would be that the silicon segregates during cooling from austenite. Silicon is known to be one of the many elements that segregate to grain boundaries to cause temper embrittlement. Although this phenomenon is usually associated with tempering of alloy steels in the range of 500-650 C, it can also occur when the steels are continuously cooled through this range [66]. Since some reaction rates are generally faster in low alloy steels such as the present, it is possible that the slow quench used provides enough time for silicon segregation during a poor quench and not during a good quench on a specimen with a high surface to volume ratio.

Another possible contributing factor is the formation of a small amount of proeutectoid ferrite during the quench. Careful microstructural examination by Koo [64] showed that this is not a major factor in the prevention of austenite nucleation at grain boundaries, however, as shown in Fig. 27b, it does occur on occasion in larger specimens.

Another important processing parameter is the amount of cold work put into the material between the two thermal treatments, i.e, between the quench to martensite and two phase annealing. This cold work could be either intentional or a consequence of handling and/or coiling of the rods.

Fig. 28a shows the structure of a 0.125 inch (3.2 mm)

diameter rod of alloy S heat treated without cold work. This structure is identical to that of alloy SV when heated in the form of a thin rod as described earlier. Cold working the martensitic rod 5% by wire drawing prior to two phase annealing breaks up the martensite particles. Prior packets are still easily identified, however, the beneficial acicular morphology is degraded. Cold working 10% almost eliminates the acicular particles resulting in a rather uniform distribution of nearly equiaxed particles.

Therefore, cold working between heat treatments should be avoided unless the specific application requires equiaxed particles as in the martensite strain ratio experiment (section 3.3.2). A typical coiling process, e.g., a 0.219 inch (5.5 mm) diameter rod coiled into a 36 inch (0.9 m) diameter, produces a maximum strain of 0.6% and should not pose any problem.

There are several possibilites for the mechanism of change from acicular to equiaxed. The requirements for the formation of acicular martensite particles are nucleation of austenite at the lath boundaries and growth along these boundaries before the boundary migrates [62]. The removal of any of these factors is sufficient to cause equiaxed particles to form. The cold work could possibly, 1) introduce nucleation sites other than the lath boundaries, 2) break up or displace the boundaries to disrupt growth along these boundaries, or 3) promote migration of these boundaries.

4.6 Optimum Design

This section describes what is thought to be the optimum design of a heat treated dual phase steel for drawing to produce high-strength wire. Based on the data in Table 7, alloy S double heat treated at 950 C has the most promising properties. It has the same drawability as the martensitic specimen and the SV alloy double heat treated at the same temperature and has a higher tensile strength than both. It is also attractive from an economic point of view since it does not contain vanadium.

The results of Table 7 show that a decrease in the volume fraction of martensite does not reduce the strength of the wire drawn to a strain of 3.6. However, it does cause a significant increase in the drawability of the wire. When the decrease in volume fraction is accomplished through use of a lower annealing temperature, the carbon content of the martensite increases, leading to an increase in the void density as discussed in section 4.1. Thus, it is recommended that a lower carbon content be used, i.e., in the range of 0.06 to 0.08 wt.%. This will improve the overall drawability-ductility-strength combinations of the wire.

The first quench should be a moderately fast quench, such as a very rapid oil quench or a poor water quench, to prevent the formation of grain boundary martensite particles. The second quench should be as rapid a quench as possible, such as an agitated iced brine quench on a specimen with a high surface to volume ratio, to reduce austenite pool shrinkage.

The drawing schedule should have at least 22% reduction in area per pass to avoid central bursting and the reductions should

not be so high as to overload the drawn wire. The drawing should always be done in the same direction. A very low drawing speed such as on a tensile test machine is ideal, however this is not practical and so the lowest speed on the drawing machine should be used. The best dies and lubricant should be used to minimize drawing load, frictional heating, and damage to the wire. The results of section 3.3.4 show that stress relief at 400 C for 3 minutes is essential.

5. CONCLUSIONS

Based on the results of this research on the microstructure-mechanical property relationships of dual phase steel and wire drawn from dual-phase steel, the following conclusions were made:

1. Dual-phase steel has promise as a starting material for drawing into high strength wire.
2. The Fe-2Si-0.1C alloy modified to 0.06-0.08C is the most promising.
3. A double heat treatment consisting of quenching from austenite to martensite followed by intercritical annealing and quenching should be used. The annealing temperature should be adjusted to yield 25-30 vol.% martensite in the final microstructure.
4. The formation of grain boundary allotriomorphs is avoided by using a moderately fast first quench in the double heat treatment schedule.
5. The second quench should be as rapid as possible to reduce austenite pool shrinkage and the resulting carbon segregation.
6. Stress relief after drawing provides a substantial increase in ductility.
7. The martensite deforms much less than the ferrite with large martensite particles deforming more than small particles.
8. Void formation during wire drawing occurs in all of the dual-phase microstructures studied and can be correlated with differences in their drawabiltiy and mechanical properties.

REFERENCES

1. S. Hayami and T. Furukawa, "A Family of High-Strength, Cold-Rolled Steels," Microalloying 75, Union Carbide Corp., New York, NY, pp. 311-21 (1977).

2. J. Y. Koo and G. Thomas, "Thermal Cycling Treatments and Microstructures for Improved Properties of Fe-0.12%C-0.5%Mn Steels," Mat. Sci. and Eng. 24, pp. 187-98 (1976).

3. M. S. Rashid, "GM 980X: A Unique High Strength Sheet Steel with Superior Formability," SAE Preprint No. 760206 (1976).

4. A. T. Davenport (ed.) Formable HSLA and Dual-Phase Steels, AIME, New York, NY (1979).

5. Production and Properties of Vanadium Dual-Phase Steels and Cold Pressing Steels in the Automobile Industry, Proc. of a Seminar, Vanadium Intl. Tech. Comm., Berlin (1978).

6. R. A. Kot and J. W. Morris (eds.), Structure and Properties of Dual-Phase Steels, AIME, New York, NY (1979).

7. R. A. Kot and B. L. Bramfitt (eds.), Fundamentals of Dual Phase Steels, AIME, New York, NY (1981).

8. B. L. Bramfitt and P. L. Mangonon, Jr. (eds.), Metallurgy of Continuous-Annealed Sheet Steel, AIME, New York, NY (1982).

9. N. J. Kim, "Design of Dual-Phase Fe/Mn/C Steel for Low Temperature Application," Ph.D. Thesis, University of California, Berkeley, LBL-12661, (1981).

10. N. V. Bangaru, "Microstructural and Micromechanical Control for Producing Ferrite-Austenite Dual Phase Structures in Low Alloy Steels," presented at the 112th Annual Mtg. of the Metallurgical Society of AIME, Atlanta, Georgia, March 6-10, 1983.

11. J. McMahon and G. Thomas, "Development of Economical, Tough, Ultra-High-Strength Fe-Cr-C Steels," The Microstructure and Design of Alloys, Proc. 3rd Intl. Conf. on Strength of Metals and Alloys 1, Inst. of Metals, London, pp. 180-83 (1973).

12. G. Thomas, "Utilization and Limitations of Phase Transformations and Microstructure in Alloy Design for Strength and Toughness," Battelle Colloquium on Fundamental Aspects of Structural Alloy Design, R. I. Jaffee and B. A. Wilcox (eds.) Plenum Publishing Co., pp. 331-58 (1977).

13. J. Y. Koo and G. Thomas, "Design of Duplex Fe/X/0.1C Steels for Improved Mechanical Properties," Met. Trans. 8A, pp. 525-28 (1977).

14. J. Y. Koo and G. Thomas, "Design of Duplex Low Carbon Steels for Improved Strenth: Weight Applications," Formable HSLA and Dual-Phase Steels, A. T. Davenport (ed.), AIME, New York, NY, pp. 40-55 (1979).

15. A. P. Coldren, G. Tither, A. Cornford, and J. R. Hiam, "Development and Mill Trial of As-Rolled Dual-Phase Steel," Formable HSLA and Dual-Phase Steels, A. T. Davenport (ed.), AIME, New York, NY, pp. 205-28 (1979).

16. G. R. Speich, V. A. Demarest, and R. L. Miller, "Formation of Austenite During Intercritical Annealing of Dual-Phase Steels," Met. Trans. 12A, pp. 1419-28 (1980).

17. P. Wycliffe, G. R. Purdy, and J. D. Embury, "Austenite Growth in the Intercritical Annealing of Ternary and Quarternary Dual-Phase Steels," Fundamentals of Dual-Phase Steels R. A. Kot and B. L. Bramfitt (eds.), AIME, New York, NY, pp. 59-83 (1981).

18. A. D. Romig, Jr. and R. Salzbrenner, "Elemental Partitioning as a Function of Heat Treatment in an Fe-Si-V-C Dual Phase Steel," Scripta Met. 16, pp. 33-38 (1982).

19. A. Nakagawa, J. Y. Koo, and G. Thomas, "Effect of Vanadium on Structure-Property Relations of Dual-Phase Fe/Mn/Si/0.1C Steels," Met. Trans. 12A, pp. 1965-72 (1981).

20. E. R. Petty (ed.), Martensite - Fundamentals and Technology, Longman Group Ltd., London (1970).

21. M. S. Rashid and E. R. Cprek, "Relationship Between Microstructure and Formability in Two High-Strength, Low Alloy Steels," Formability Topics-Metallic Materials, ASTM STP 647, B. A. Niemeier, A. K. Schmieder and J. R. Newby (eds.) ASTM, pp. 174-90 (1978).

22. R. G. Davies, "Influence of Martensite Composition and Content on the Properties of Dual-Phase Steels," Met. Trans. 9A, pp. 671-79 (1978).

23. J. Y. Koo, M. J. Young, and G. Thomas, "On the Law of Mixtures in Dual Phase Steels," Met. Trans. 11A, pp. 852-54 (1980).

24. G. R. Speich and R. L. Miller "Mechanical Properties of Ferrite Martensite Steels," Structure and Properties of Dual-Phase Steels, R. A. Kot and J. W. Morris (eds.), AIME, New York, NY, pp. 145-82 (1979).

25. P. K. Costello, "Design of Duplex Low-Carbon Steels with Carbide Forming Elements," M. S. Thesis, University of California, Berkeley, LBL-8628, (1978).

26. R. H. Hoel and G. Thomas, "Ferrite Structure and Mechanical Properties of Low Alloy Duplex Steels," Scripta Met. 15, pp. 867-72 (1981).

27. J. S. Gau, J. Y. Koo, A. Nakagawa, and G. Thomas, "Microstructure and Properties of Dual-Phase Steels Containing Fine Precipitates," Fundamentals of Dual-Phase Steels, R. A. Kot and B. C. Bramfitt (eds.), AIME, New York, NY, pp. 47-58 (1981).

28. H. E. McGannon (ed.), The Making, Shaping and Treating of Steel, 9th ed. United States Steel, Pittsburg, PA (1971).

29. W. C. Leslie, The Physical Metallurgy of Steels, McGraw-Hill, New York, NY (1981).

30. J. D. Embury and R. M. Fisher, "The Structure and Properties of Drawn Pearlite," Acta Met. 14, pp. 147-59 (1966).

31. J. D. Embury, A. S. Keh, and R. M. Fisher, "Substructural Strengthening in Materials Subject to Large Plastic Strains," Trans. TMS-AIME 236, pp. 1252-60 (1966).

32. W. F. Hosford, Jr. "Microstructural Changes During Deformation of [011] Fiber-Textured Metals," TMS-AIME 230, pp. 12-15 (1964).

33. J. F. Peck and D. A. Thomas, "A Study of Fibrous Tungsten and Iron," TMS-AIME 221, pp. 1240-46 (1961).

34. G. Langford, "A Study of the Deformation of Patented Steel Wire," Met. Trans. 1, pp. 465-77 (1970).

35. G. Langford, "Deformation of Pearlite," Met. Trans. 8A, pp. 861-75 (1977).

36. D. A. Porter, K. E. Easterling, and G. D. W. Smith, "Dynamic Studies of the Tensile Deformation and Fracture of Pearlite," Acta Met. 26, pp. 1405-22 (1978).

37. A. S. Argon, J. Im, and R. Safoglu, "Cavity Formation from Inclusions in Ductile Fracture," Met. Trans. 6A, pp. 825-37 (1975).

38. J. R. Fisher and J. Gurland, "Void Nucleation in Spherodized Carbon Steels - Part 2: Model," Met. Sci. 15, pp. 193-202 (1981).

39. J. R. Fisher and J. Gurland, "Void Nucleation in Spherodized Carbon Steels - Part 1: Experimental," Met. Sci. 15, pp. 185-92 (1981).

40. A. F. Szewczyk and J. Gurland, "A Study of the Deformation and Fracture of a Dual-Phase Steel," Met. Trans. 13A, pp. 1821-26 (1982).

41. G. E. Dieter, Jr., Mechanical Metallurgy, McGraw-Hill, New York, NY (1961).

42. F. A. McClintock, "A Criterion for Ductile Fracture by the Growth of Holes," J. Appl. Mech., 35, pp. 363-67 (1968).

43. D. A. Korzekwa, R. D. Lawson, D. K. Matlock, and G. Krauss, "A Consideration of Models Describing the Strength and Ductility of Dual-Phase Steels," Scripta Met. 14, pp. 1023-28 (1980).

44. J. Y. Koo and G. Thomas, "Developments in Strong, Ductile Duplex Ferritic-Martensitic Steels," Structure and Properties of Dual-Phase Steels, R. A. Kot and J. W. Morris (eds), AIME, New York, NY, pp. 183-201 (1979).

45. N. J. Kim and G. Thomas, "Effects of Morphology on the Mechanical Behavior of a Dual Phase Fe/2Si/0.1C Steel," Met. Trans 12A, pp. 483-89 (1981).

46. E. C. Bain and H. W. Paxton, Alloying Elements in Steel, Amer. Soc. for Metals, Metals Park, Ohio (1966).

47. G. Langford, P. K. Nagata, R. J. Sober, and W. C. Leslie, "Plastic Flow in Binary Substitutional Alloys of BCC Iron-Effects of Wire Drawing and Alloy Content on Work Hardening and Ductility," Met. Trans. 3, pp. 1843-49 (1972).

48. E. E. Underwood, "Applications of Quantitative Metallography," ASM Metals Handbook, 8th ed., 8, pp. 37-47 (1973).

49. D. K. Matlock, G. Krauss, L. F. Ramos, and G. S. Huppi, "A Correlation of Processing Variables with Deformation Behavior of Dual-Phase Steels," Structure and Properties of Dual-Phase Steels, R. A. Kot and J. W. Morris (eds.), AIME, New York, NY, pp. 62-90 (1979).

50. R. D. Lawson, D. K. Matlock, and G. Krauss, "An Etching Technique for Microalloyed Dual-Phase Steels," Metallography 13, pp. 71-87 (1980).

51. H. Majors, Jr., "Studies in Cold Drawing - Part 1: Effect of Cold Drawing on Steel," Trans. ASME 77, pp. 37-48 (1955).

52. W. T. Read, Jr., Dislocations in Crystals, McGraw-Hill, New York, NY (1953).

53. N. P. Suh and A. P. L. Turner, Elements of the Mechanical Behavior of Solids, McGraw-Hill, New York, NY (1975).

54. B. Avitzur, "New, Improved Criterion for the Prevention of Central Burst in Wire Drawing and Extrusion," Wire Journal 1, pp. 77-86 (1974).

55. R. M. Caddell and A. G. Atkins, "Optimum Die Angles and Maximum Attainable Reductions in Rod Drawing," Trans. ASME, Journal of Engineering for Industry, Series B 91, pp. 664-72 (1969).

56. W. A. Backofen, Deformation Processing, Addison-Wesley, Reading, Mass. (1972).

57. J. A. Schey, Introduction to Manufacturing Processes, McGraw-Hill, New York, NY (1977).

58. J. I. Kim, C. K. Syn, and J. W. Morris, Jr., "Microstructural Sources of Toughness in QLT-Treated 5.5 Ni Cryogenic Steel," Met. Trans. 14A, pp. 93-103 (1983).

59. J. H. Ahn, "Effect of Grain Size on Mechanical Properties of Dual-Phase Fe/2Si/.1C Steels," M.S. Thesis, University of California, Berkeley, in press.

60. A. R. Marder and G. Krauss, "The Morphology of Martensite in Iron-Carbon Alloys," Trans. ASM 60, pp. 651-60 (1967).

61. J. Y. Koo and G. Thomas, "Lattice Imaging of Twin, Lath and Martensite Boundaries in Duplex Low Carbon Steels," 35th Annual Proc. of EMSA, G. W. Bailey (ed.), Claitor's Publishing Division, Boston, MA, pp. 118-19 (1975).

62. M. R. Plichta and H. I. Aaronson, "Influence of Alloying Elements upon the Morphology of Austenite Formed from Martensite in Fe-C-X Alloys," Met. Trans. 5, pp. 2611-13 (1974).

63. B. V. Karlekar and R. M. Desmond, Engineering Heat Transfer, West Publishing Co., St. Paul, Minn. (1977).

64. J. Y. Koo "Design of Duplex Low Carbon Steels for Improved Strength: Weight Applications," Ph.D. Thesis, University of California, Berkeley, LBL-6657 (1977).

65. K. J. Irvine and F. B. Pickering, "Low Carbon Steels with Ferrite-Pearlite Structures," JISI 204, pp. 944-59 (1963).

66. R. W. K. Honeycombe, Steels - Microstructure and Properties, Amer. Soc. for Metals, Metals Park, Ohio (1982).

Table 1. Alloy Compositions

Alloy Designation	Element (wt.%)							
	C	Si	Mn	P	S	Al	V	Fe
SV	0.10	1.74	0.009	0.005	<0.005	0.01	0.09	bal.
S	0.09	2.01	0.009	0.005	<0.005	0.01	-	bal.
M	0.10	-	1.55	0.005	0.003	0.02	-	bal.

Table 2. Martensite Volume Fractions

Alloy	Heat Treatment	Annealing Temperature (C)	Volume percent Martensite	%C in Martensite*
SV	Double	850	14 ± 4	0.71
		950	28 ± 8	0.36
		960	36 ± 6	0.28
		1000	53 ± 12	0.19
		1050	94 ± 3	0.11
SV	Single	950	27 ± 8	0.37
		1150	100	0.10
S	Double	950	36 ± 7	0.28
M	Double	757	27 ± 9	0.37

* Estimated from the volume fraction and bulk carbon content.

Table 3. Void Density at $\varepsilon = 3.6$

Specimen	Voids/mm^2
SV DBL 850	1400
SV DBL 950	240
SV DBL 1000	83
SV SING 1150	62
SV SING 950	360

Table 4. Martensite Strain Ratio

Total Wire Strain	Total Wire Aspect Ratio	Small Particles (2 - 10 μm)			Large Particles (10 - 30 μm)		
		Aspect Ratio	Strain ε	$\frac{\varepsilon_{MS}}{\varepsilon_T}$	Aspect Ratio	Strain ε	$\frac{\varepsilon_{MS}}{\varepsilon_T}$
0	0	1.6 (1.0)*	0	0	1.6 (1.0)	0	0
1.01	4.5	~1.6 (0)	0	0	3.5 (2.2)	0.52	0.52
1.94	18	~1.6 (0)	0	0	7.5 (4.7)	1.03	0.53
3.01	96	2.6 (1.6)	0.32	0.11	**	-	-

* Numbers in parentheses are corrected for the inital aspect ratio of the particles.

** Too large to measure.

Table 5. Tensile Test Summary (As Heat Treated)

Specimen	Yield ksi (MPa)	Tensile ksi (MPa)	Elongation (%) Uniform	Elongation (%) Total	RA (%)
SV DBL 850	74 ± 1 (510 ± 7)	113 ± 1 (780 ± 7)	13 ±0.5	25 ±1.1	50 ±2
SV DBL 950	78 ± 2 (540 ± 8)	119 ± 1 (820 ± 8)	13 ±0.2	27 ±0.4	56 ±1
SV DBL 1000	93 ± 3 (640 ± 15)	128 ± 1 (880 ± 8)	10 ±1.7	22 ±3.3	57 ±2
SV SING 950	94 ± 4 (650 ± 28)	130 ± 2 (900 ± 11)	10 ±0.5	18 ±0.7	39 ±1
SV SING 1150	143 ± 2 (1000 ± 20)	167 ± 2 (1150 ± 13)	5 ±0.2	17 ±1.8	64 ±4
S DBL 950	77 ± 1 (530 ± 8)	120 ± 2 (830 ± 15)	14 ±0.2	25 ±0.8	51 ±3
M DBL 757	63 ± 3 (430 ± 18)	100 ± 1 (690 ± 10)	13 ±1.5	21 ±1.7	39 ±1

Table 6. Drawability Ranking

Rank	Specimen	Minimum Diameter (in)	Strain	Maximum Vickers Hardness	Volume Percent Martensite
1	SV DBL 850	<0.0095	>6.1	499 ± 9*	14 ± 4
2	SV DBL 950	0.0095	6.1	547 ± 6*	28 ± 8
2	SV SING 1150	0.0095	6.1	651 ± 6	100
2	S DBL 950	0.0095	6.1	580 ± 7	36 ± 7
3	S DBL 1000	0.0136	5.4	577 ± 11	53 ± 12
4	SV SING 950	0.0330	3.6	500 ± 7	27 ± 8
5	M DBL 950	0.0370	3.4	438 ± 11	27 ± 9

* Maximum hardness at d = 0.0136 in, ε = 5.4.

Table 7. Mechanical Properties of Drawn Wire at $\varepsilon = 3.6$

Specimen	Vickers Hardness 1000g load	Tensile Strength	
		ksi	MPa
SV DBL 850	461 ± 10	279 ± 5	1920 ± 34
SV DBL 950	460 ± 8	276 ± 9	1900 ± 62
SV DBL 1000	508 ± 7	254 ± 3	1750 ± 21
SV SING 950	500 ± 7	*	*
SV SING 1150	601 ± 12	292 ± 4	2010 ± 28
S DBL 950	496 ± 10	313 ± 7	2100 ± 48

* Not tested

Table 8. Effect of Drawing Speed

Mechanical Property	Low Speed	High Speed
Vickers Hardness 1000g load	391 ± 8	377 ± 6
Tensile Strength ksi (MPa)	218 ± 4 (1503 ± 28)	206 ± 1 (1420 ± 7)
Reduction in Area (%)	37 ± 5	28 ± 12

Table 9. Effect of Stress Relief

Mechanical Property	As-Drawn	Stress Relieved 400 C, 3 min.
Tensile Strength ksi (MPa)	284 (1960)	276 (1900)
Percent Reduction in Area	~0	54
Torsional Ductility Twists in 4 inches	20	31

FIGURE CAPTIONS

Fig. 1. Stress strain curves for a Fe/Mn/Si/V/0.1C Steel with dual-phase microstructures of two different martensite volume fractions, and with a ferrite-pearlite microstructure [19].

Fig. 2. Schematic of heat treatments.

Fig. 3. Subsize cylindrical tensile test specimen.

Fig. 4. Initial dual-phase microstructures. Double heat treated alloy SV annealed at [a] 850 C, [b] 950 C, [c] 1000 C. [d] Single heat treated alloy SV, 950 C, [e] Double heat treated alloy S, 950 C. [f] Double heat treated alloy M, 757 C. Optical micrographs, 2% Nital etch.

Fig. 5. Transmission electron micrograph of the lath martensite second phase in the silicon containing alloys.

Fig. 6. Microdiffraction of double heat treated alloy SV showing the orientation of a martensite particle (B) and sub grains of the ferrite matrix (A,C and D).

Fig. 7. Scanning electron micrograph of the drawn structure at $\varepsilon = 3.6$. [a] SV DBL 850. [b] SV DBL 950. [c] SV DBL 1000. [d] SV SING 950. [e] SV SING 1150. 2% Nital etch.

Fig. 8. Variation of void density with the estimated martensite carbon content at a strain of 3.6.

Fig 9. Two surface fractograph of a drawing failure. Single heat treated alloy SV, $\varepsilon = 3.7$, scanning electron micrograph, polished surface etched with 2% Nital.

Fig. 10. Deformation of martensite as a function of strain. [a] As-heat treated, $\varepsilon = 0$. [b] $\varepsilon = 1$. [c] $\varepsilon = 2$. [d] $\varepsilon = 3$. Scanning electron micrographs, alloy S, 2% Nital etch.

Fig. 11. Transmission electron micrograph of the cell structure found in the ferrite at a strain of 3.7.

Fig. 12. Transmission electron micrograph of highly deformed ferrite flowing around a non-deforming martensite particle. $\varepsilon = 3.7$, Single heat treated.

Fig. 13. Axial transmission electron micrograph of a non-deforming martensite particle. Double heat treated alloy SV, $\varepsilon = 3.6$.

Fig. 14. Transmission electron micrograph of drawn dual-phase steel showing [110] wire texture. $\varepsilon = 3.7$.

Fig. 15. Axial section of drawn dual-phase steel. Optical micrograph, $\varepsilon = 1.6$, 2% Nital etch.

Fig. 16. Axial transmission electron micrograph of drawn dual-phase steel. Double heat treated alloy SV, $\varepsilon = 3.6$.

Fig. 17. Hardness as a function of strain for different volume fractions of martensite. Double heat treated alloy SV.

Fig. 18. Transmission electron micrograph of the ferrite/martensite interface showing a region of microtwinned martensite. Single heat treated alloy S.

Fig. 19. Transmission electron micrographs of an austenite pool that has partially transformed to ferrite plus carbide. [a] Bright field. [b]. Dark field.

Fig. 20. Composite optical micrograph of central bursting as a result of light reductions. $\varepsilon = 1.2$, alloy SV, un-etched.

Fig. 21. Photograph of wires subjected to torsional strain. [a] Un-stress relieved. [b] Stress relieved at 400 C.

Fig. 22. Scanning electron micrograph of the fracture surface of a torsion test specimen. Alloy SV, double heat treatment, stress relieved at 400 C.

Fig. 23. Schematic of the velocity fields in the wire in the die under central burst conditions.

Fig. 24. Optical micrograph showing the direct relationship between features in the dual-phase microstructure, [a], with the martensite laths and packets in the initial martensite microstructure, [b]. Double heat treated alloy S, 2% Nital etch.

Fig. 25. Optical micrographs showing the effect of specimen size/heating-cooling rates on the microstructure. [a] Thin rod, fast heating and cooling. [b] Block specimen, slow heating and cooling. Alloy SV, 2% Nital etch.

Fig. 26. Optical micrograph showing the effect of the heating rate to the two phase annealing temperature. [a] Very fast. [b] Very slow. Alloy SV, 2% Nital etch.

Fig. 27. Optical micrographs of specimens given a moderately rapid quench from austenite. [a] Subsequently two phase annealed and followed by rapid quench. [b] As quenched microstructure showing the occasional proeutectiod ferrite at the prior austenite grain boundaries. Alloy SV, 2% Nital etch.

Fig. 28. Effect of cold work prior to two phase annealing in double heat treated alloy S. [a] No deformation. [b] 5% reduction. [c] 10% reduction. Optical micrographs, 2% Nital etch.

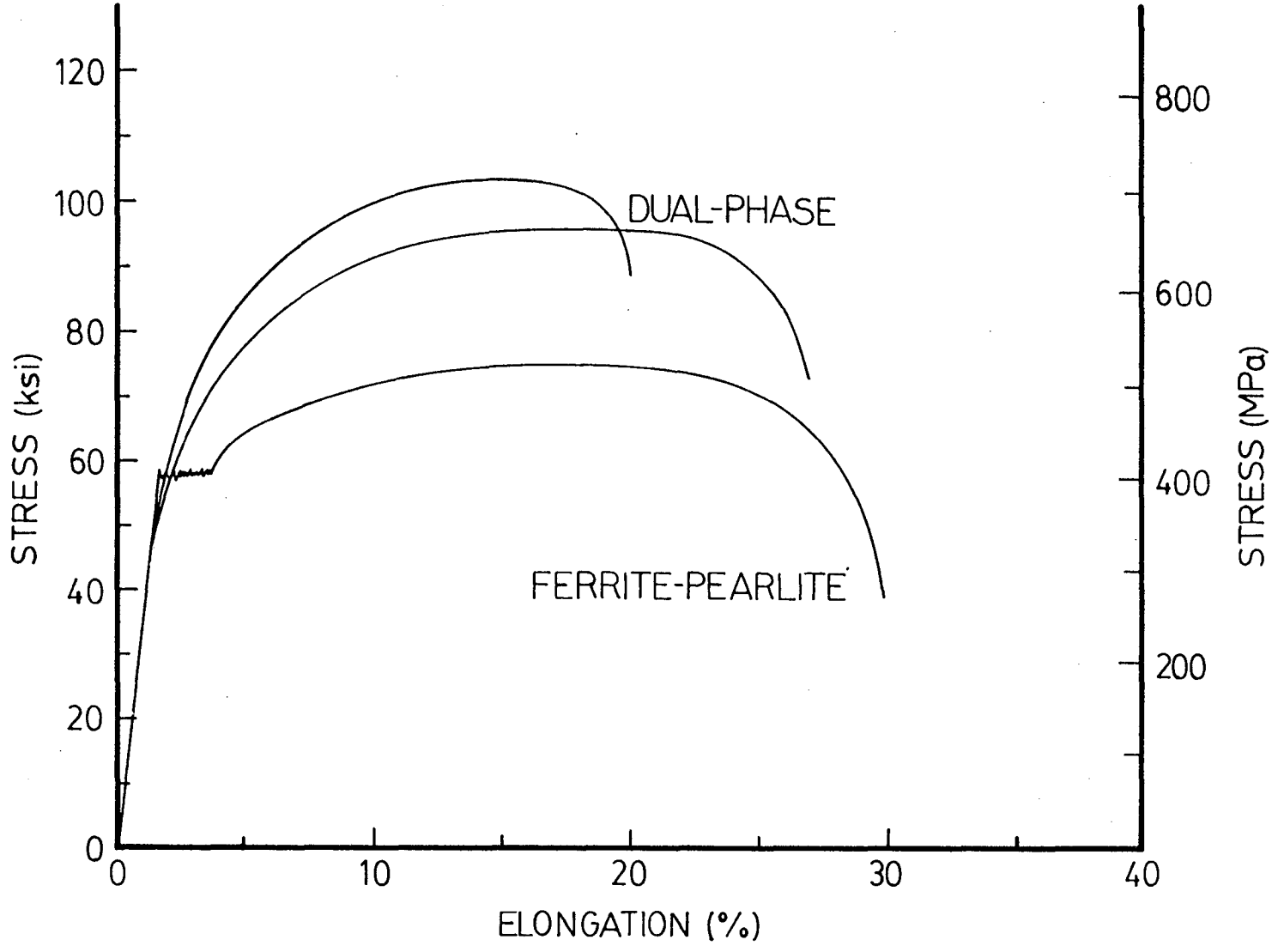

Fig. 1

XBL 838-11019

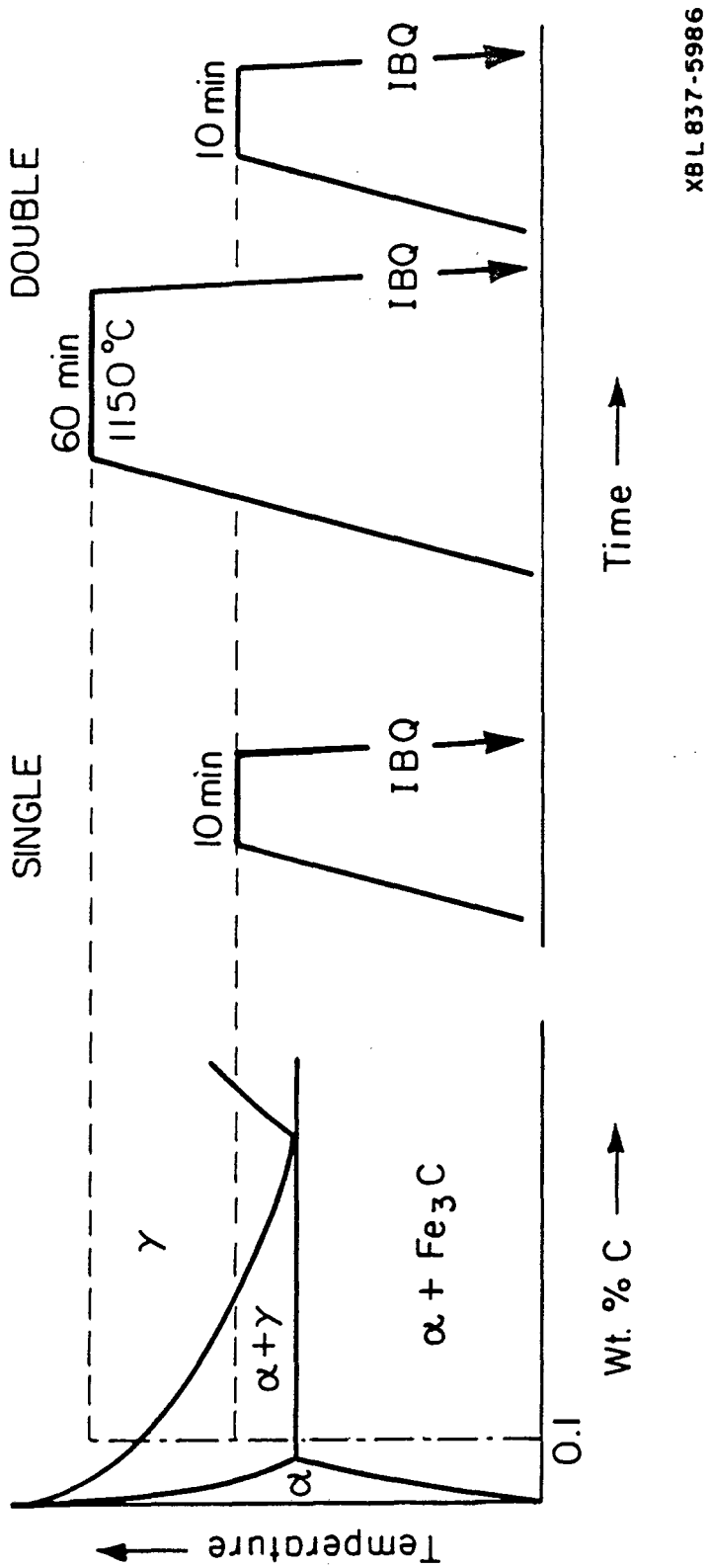

XBL 837-5986

Fig. 2

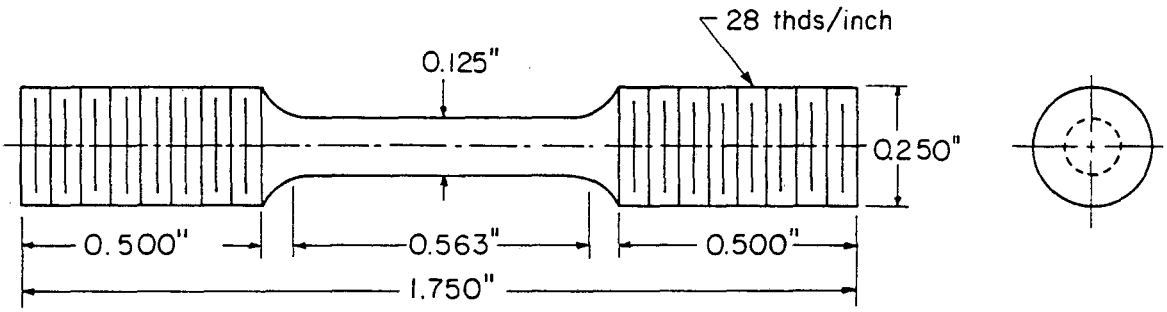

XBL 774-5354

Fig. 3

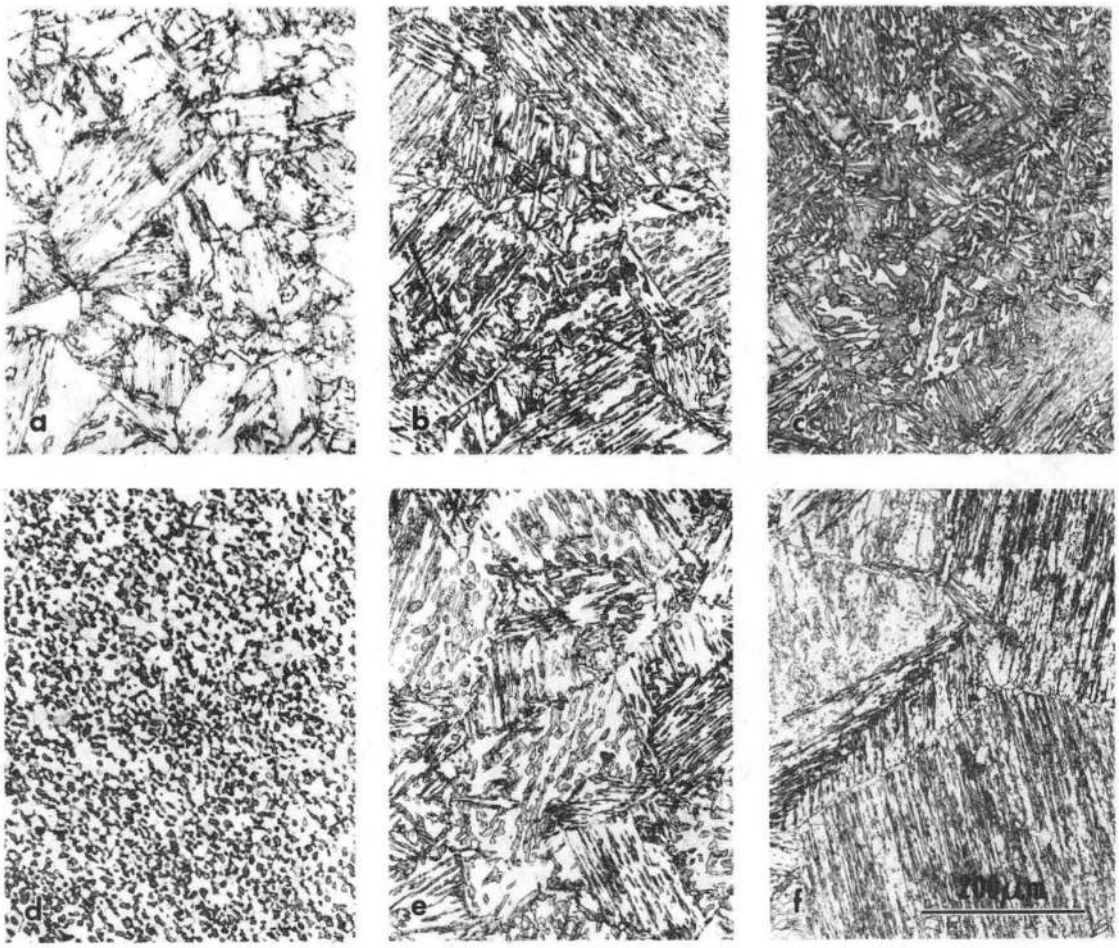

Fig. 4

XBB 837-6004

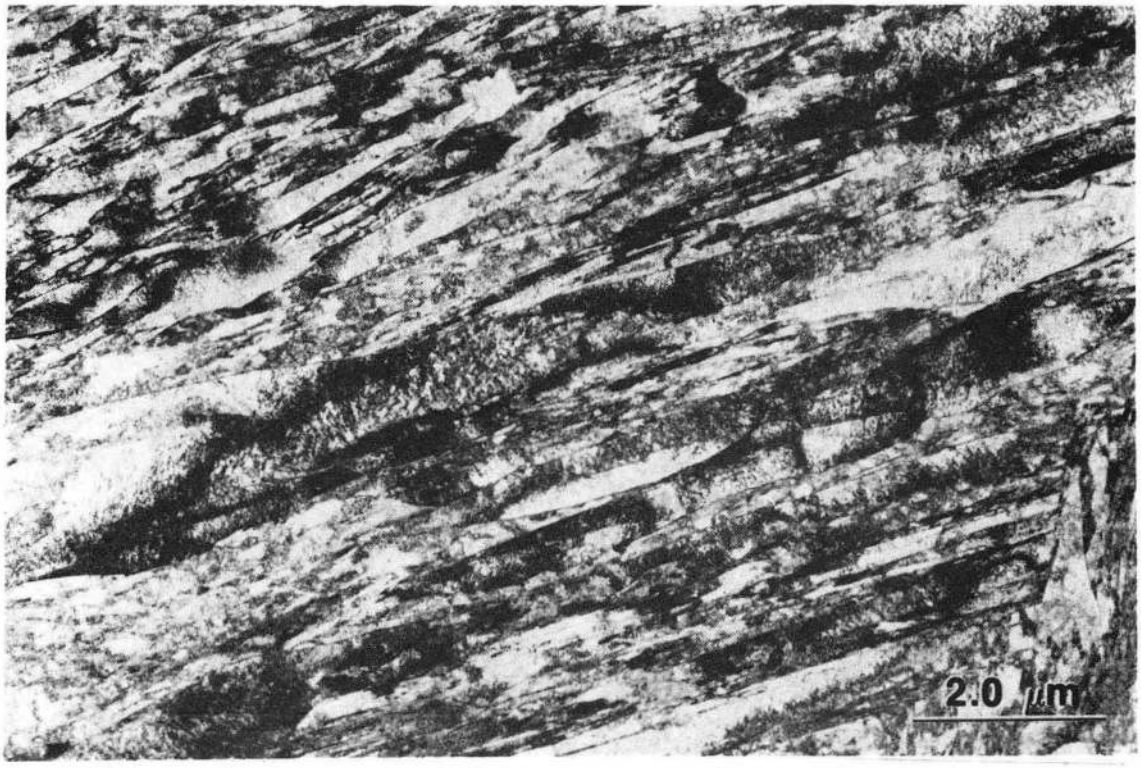

XBB 824-3481

Fig. 5

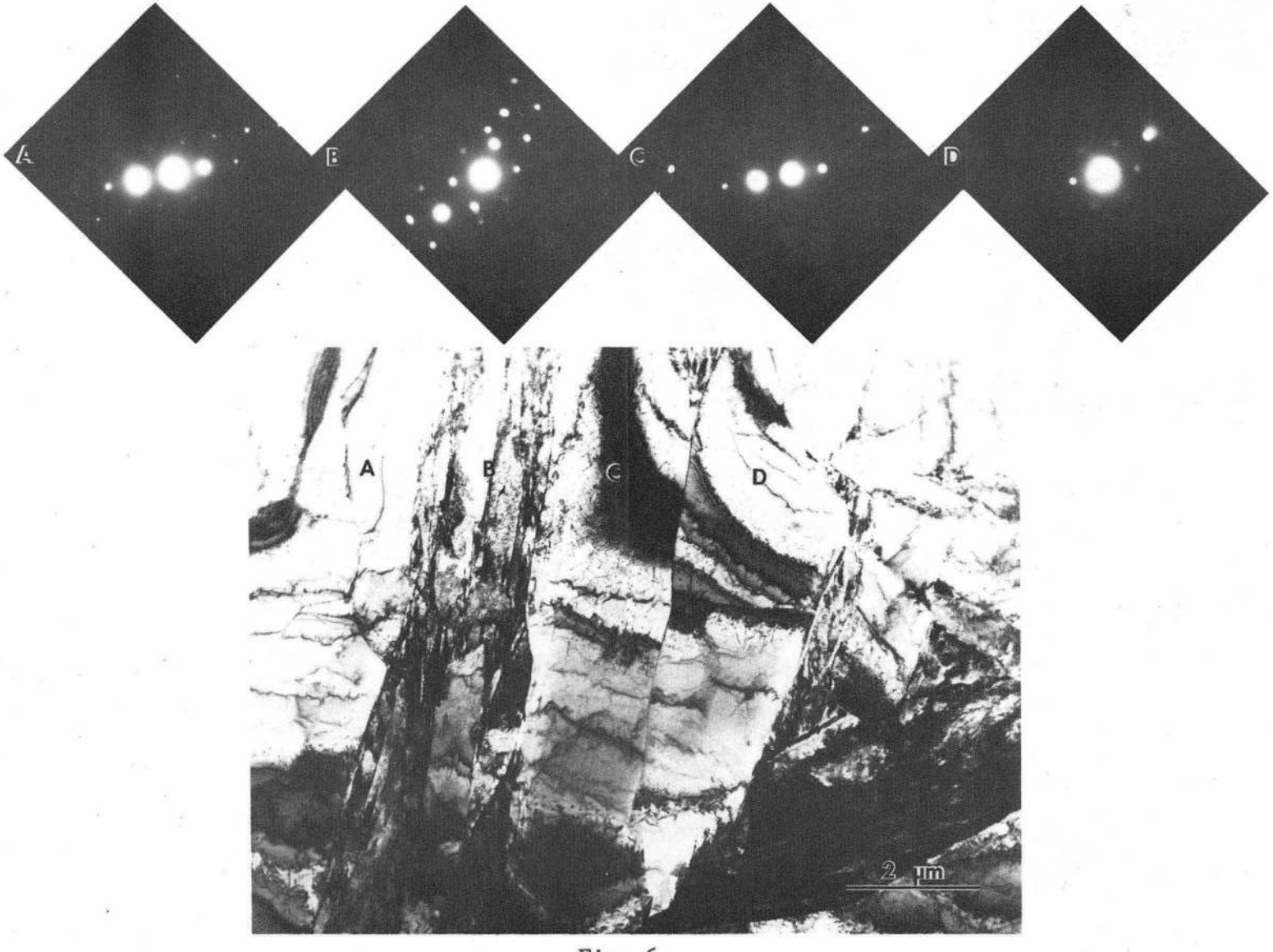

Fig. 6

XBB 836-5374

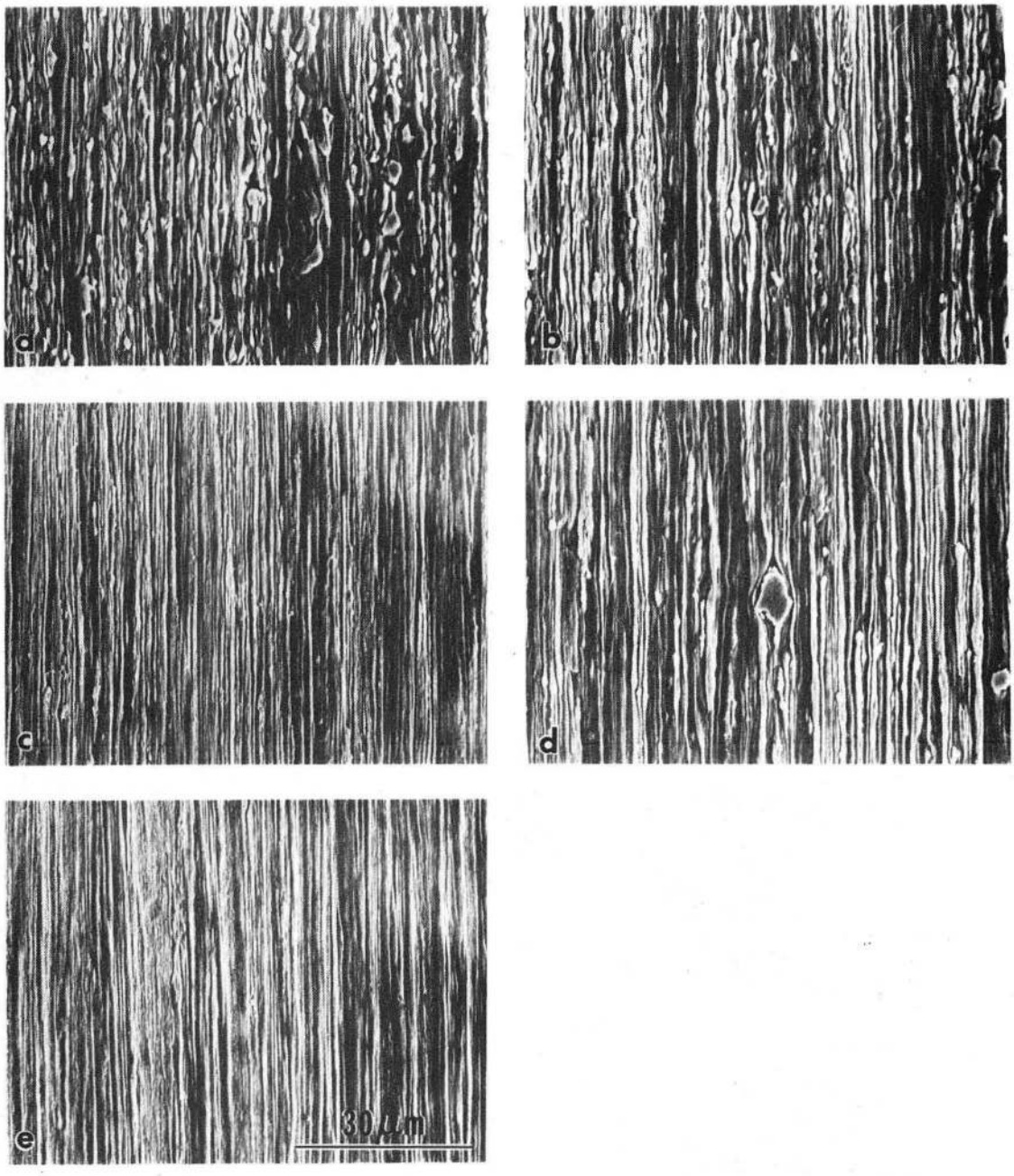

Fig. 7

XBB 837-6005

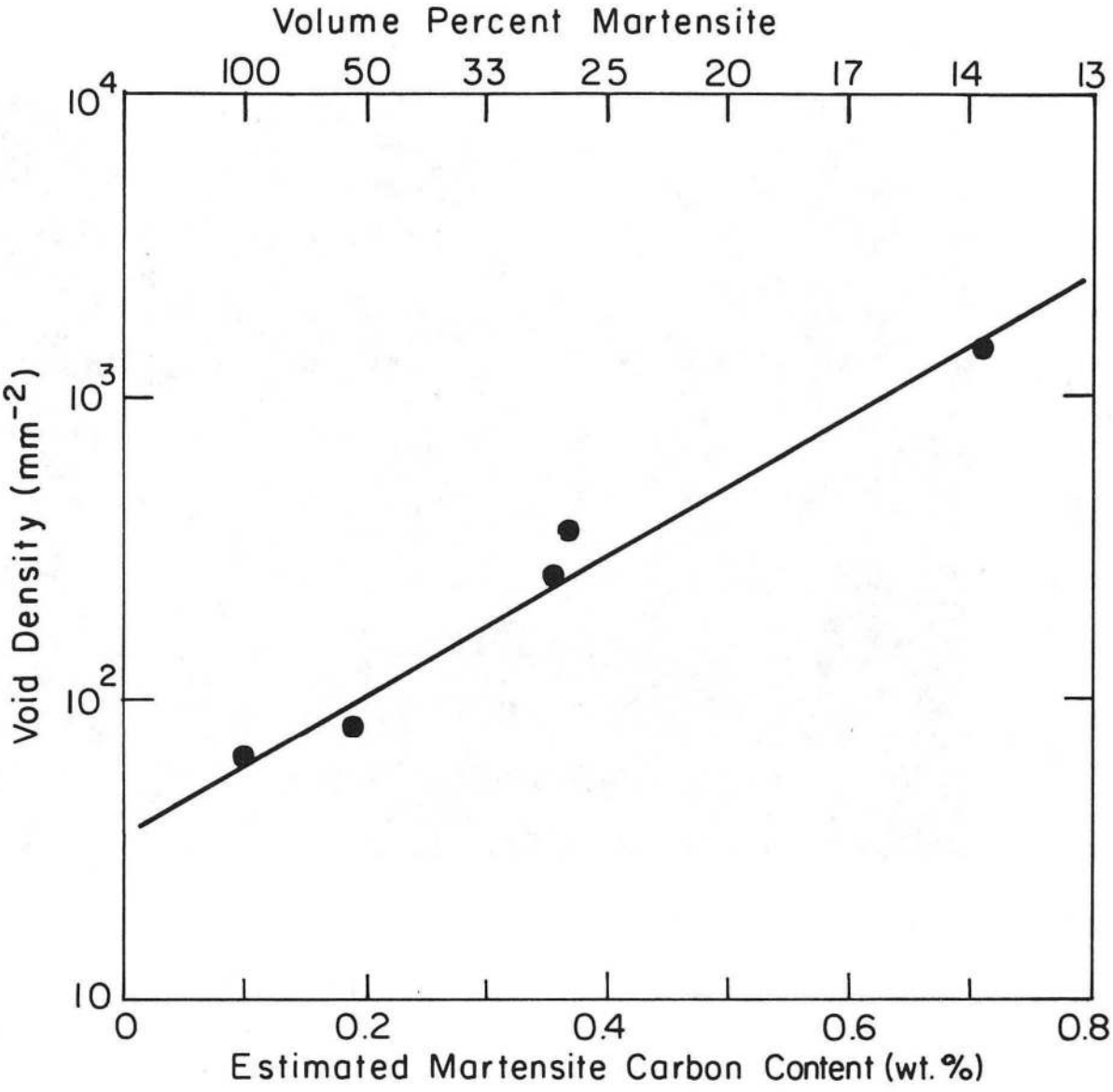

XBL838-6147

Fig. 8

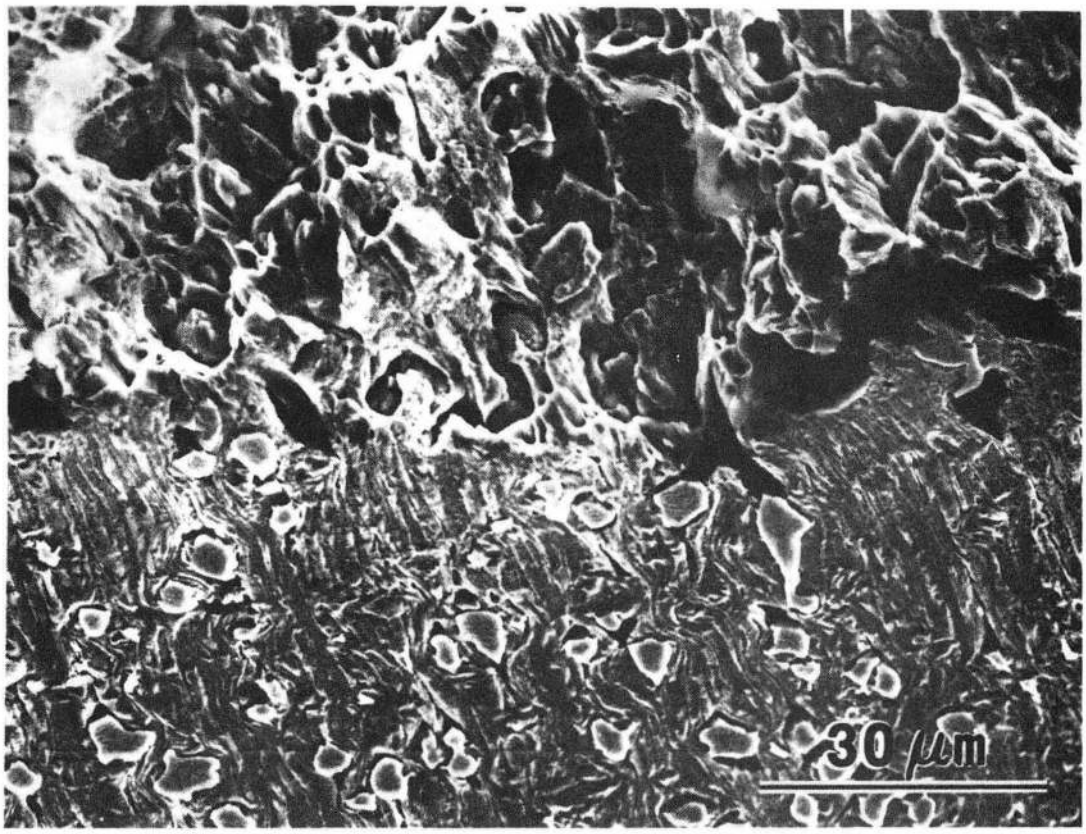

Fig. 9

XBB 838-6862

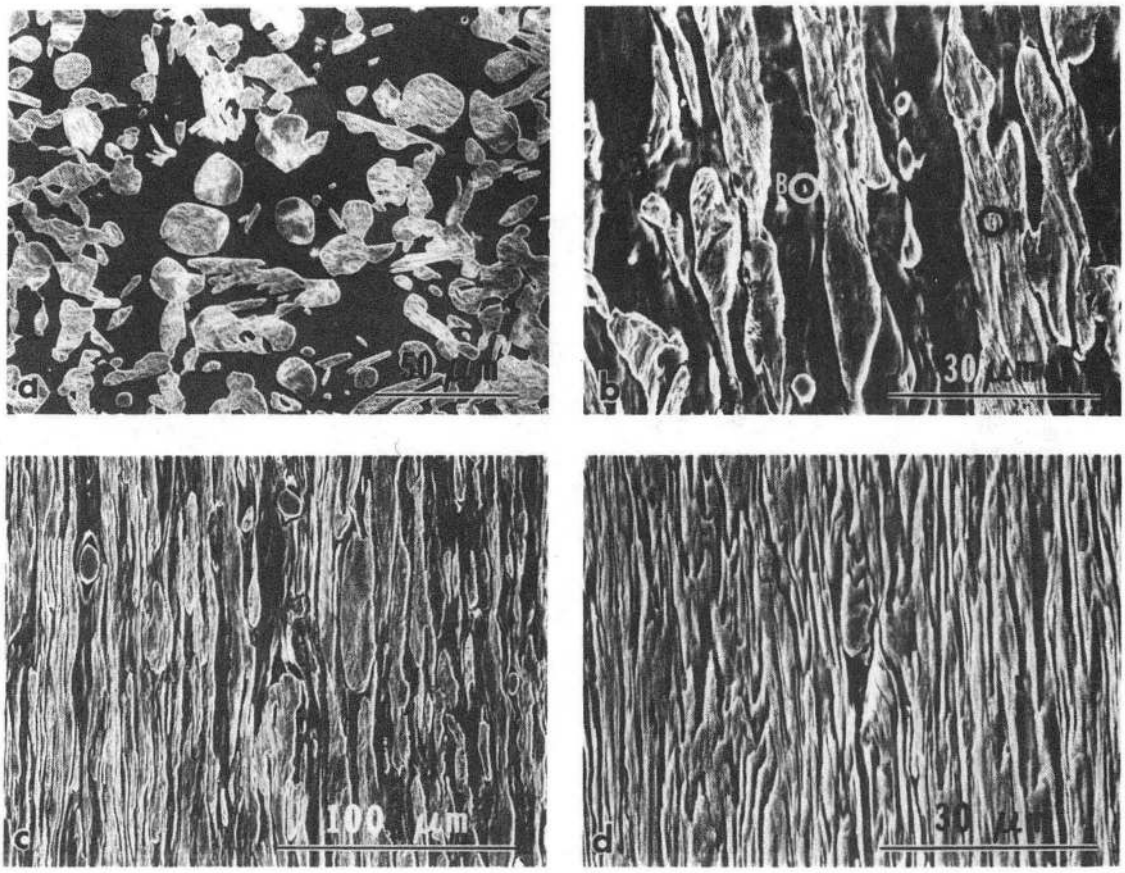

Fig. 10

XBB 837-6007

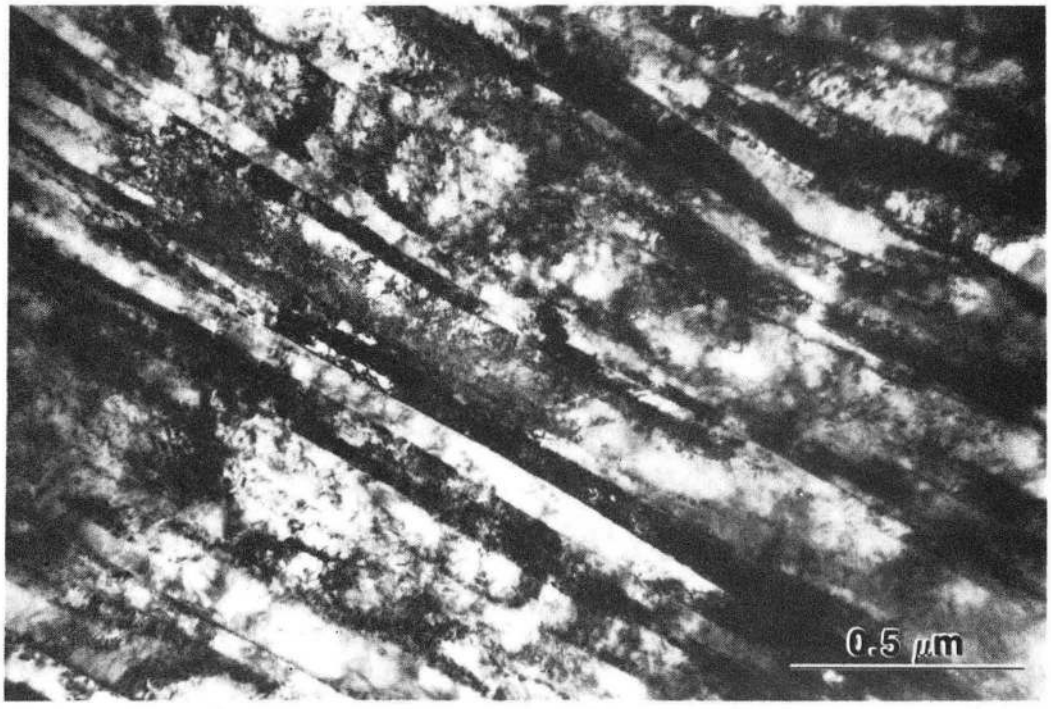

Fig. 11 XBB 823-2272

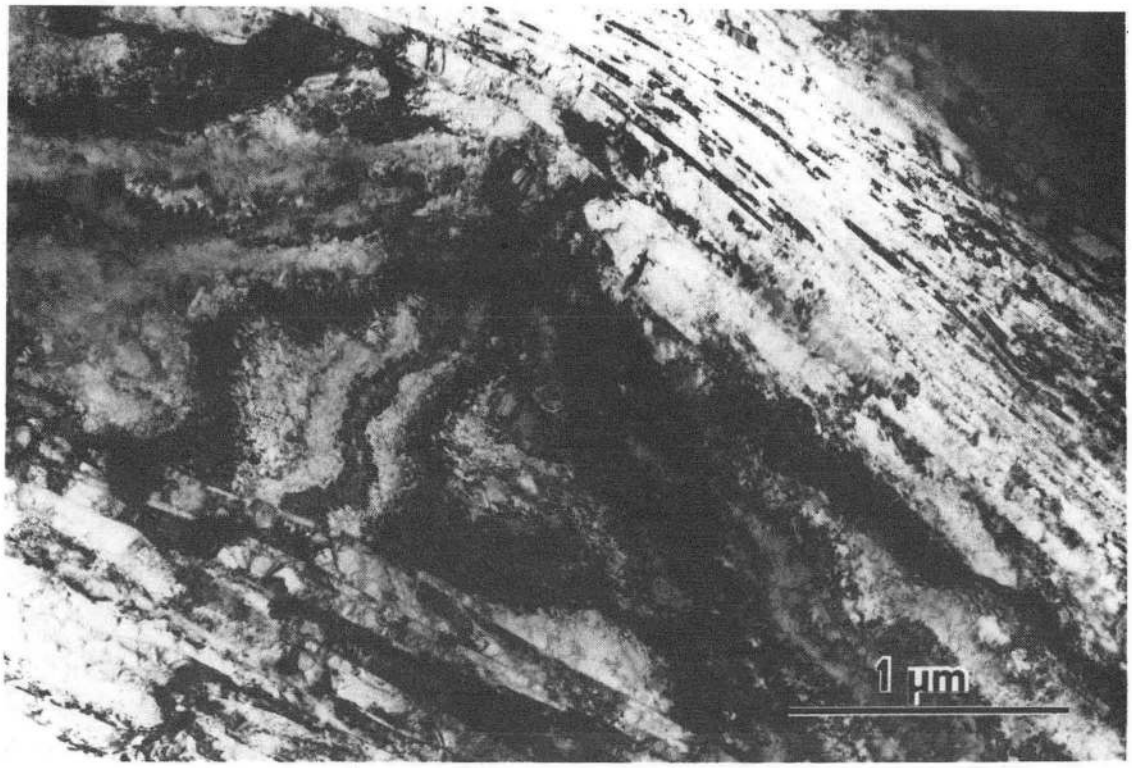

Fig. 12

XBB 820-8701

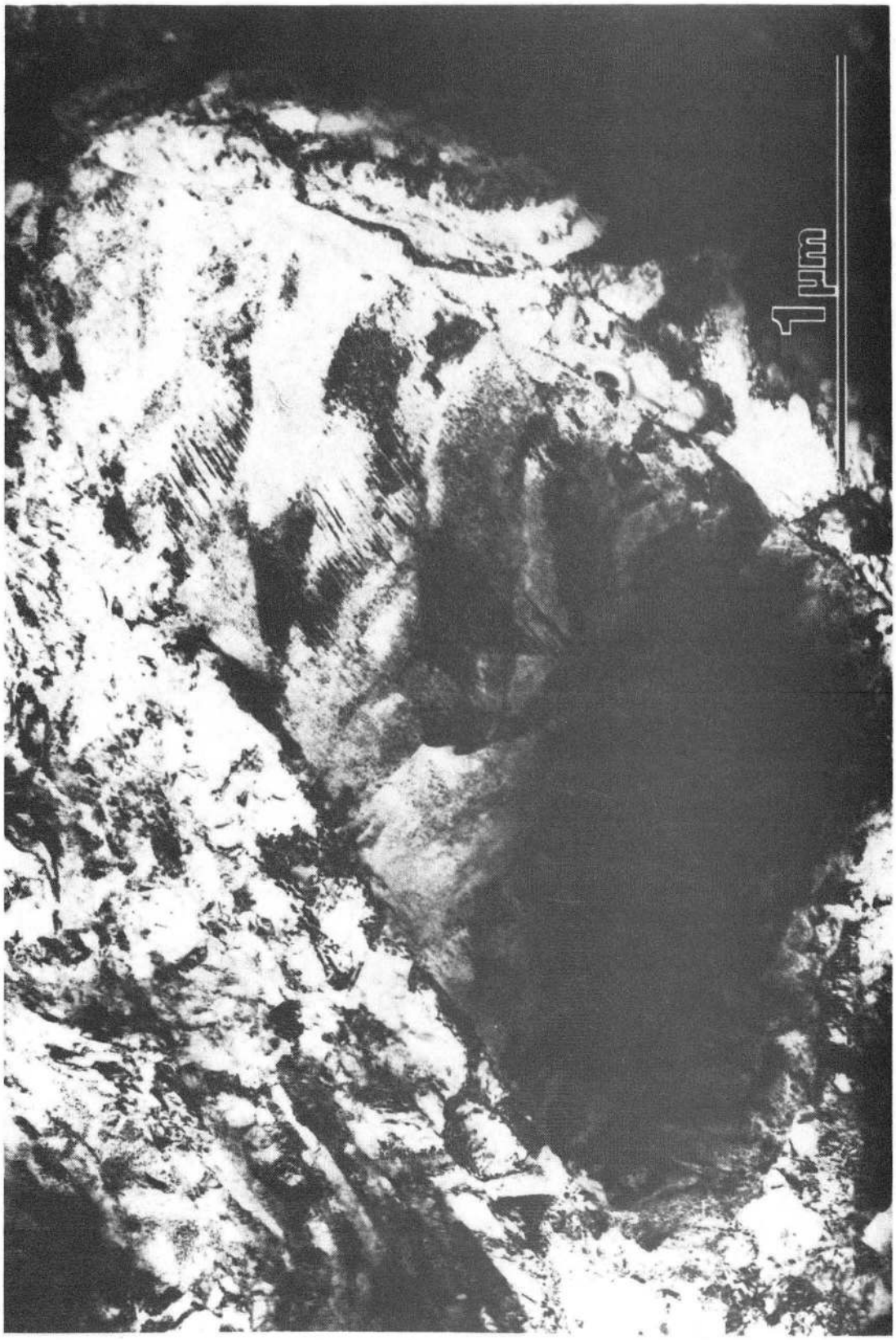

XBB 838-6986

Fig. 13

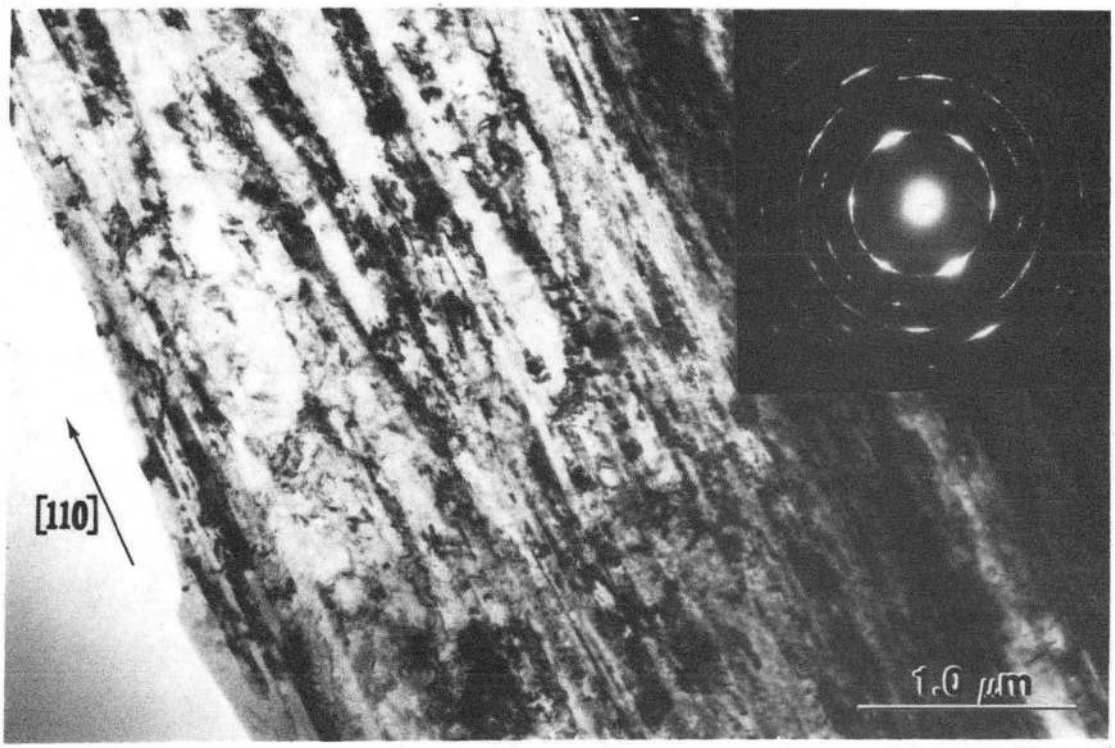

Fig. 14

XBB 824-3482

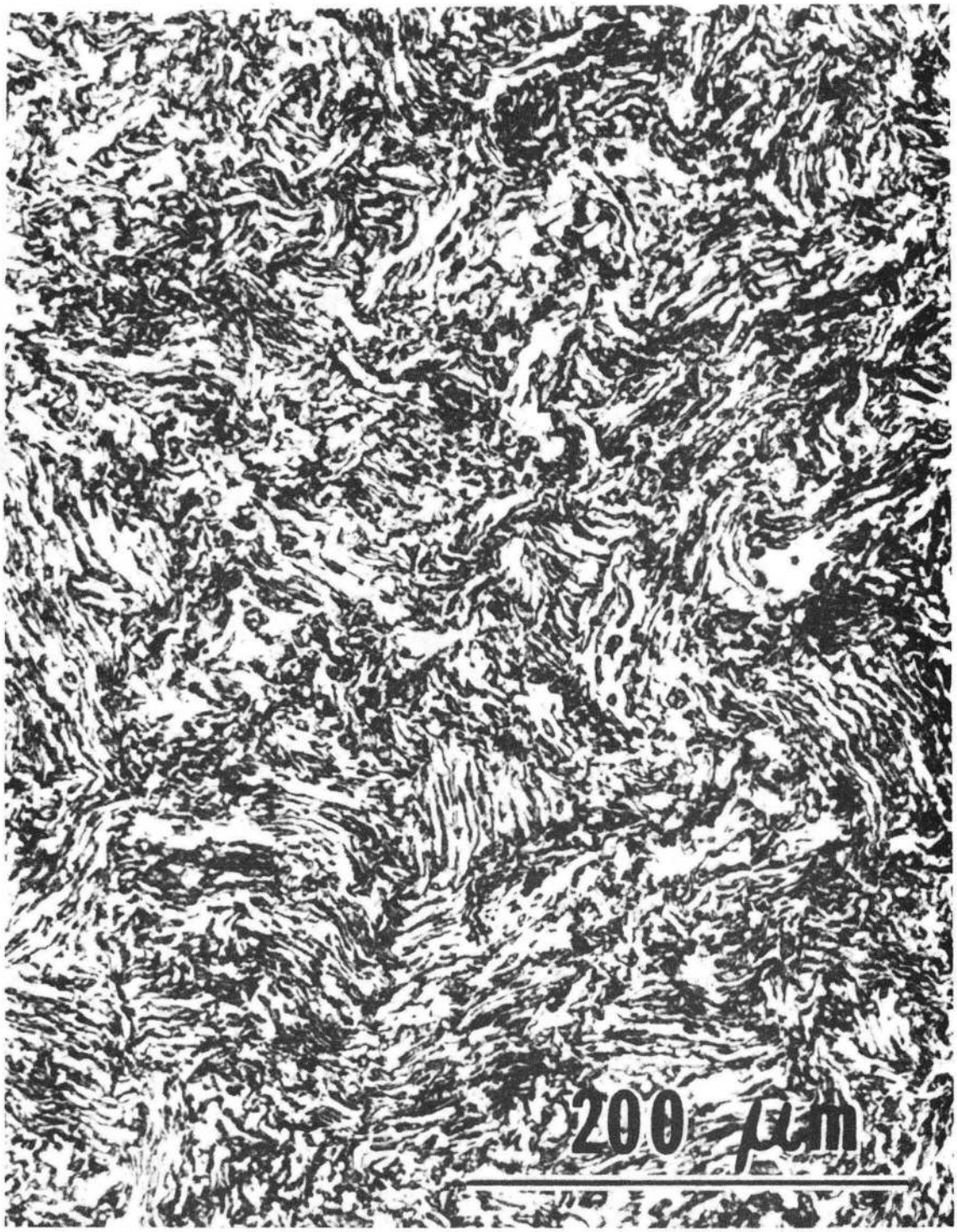

Fig. 15

XBB 837-6002

XBB 838-6985

Fig. 16

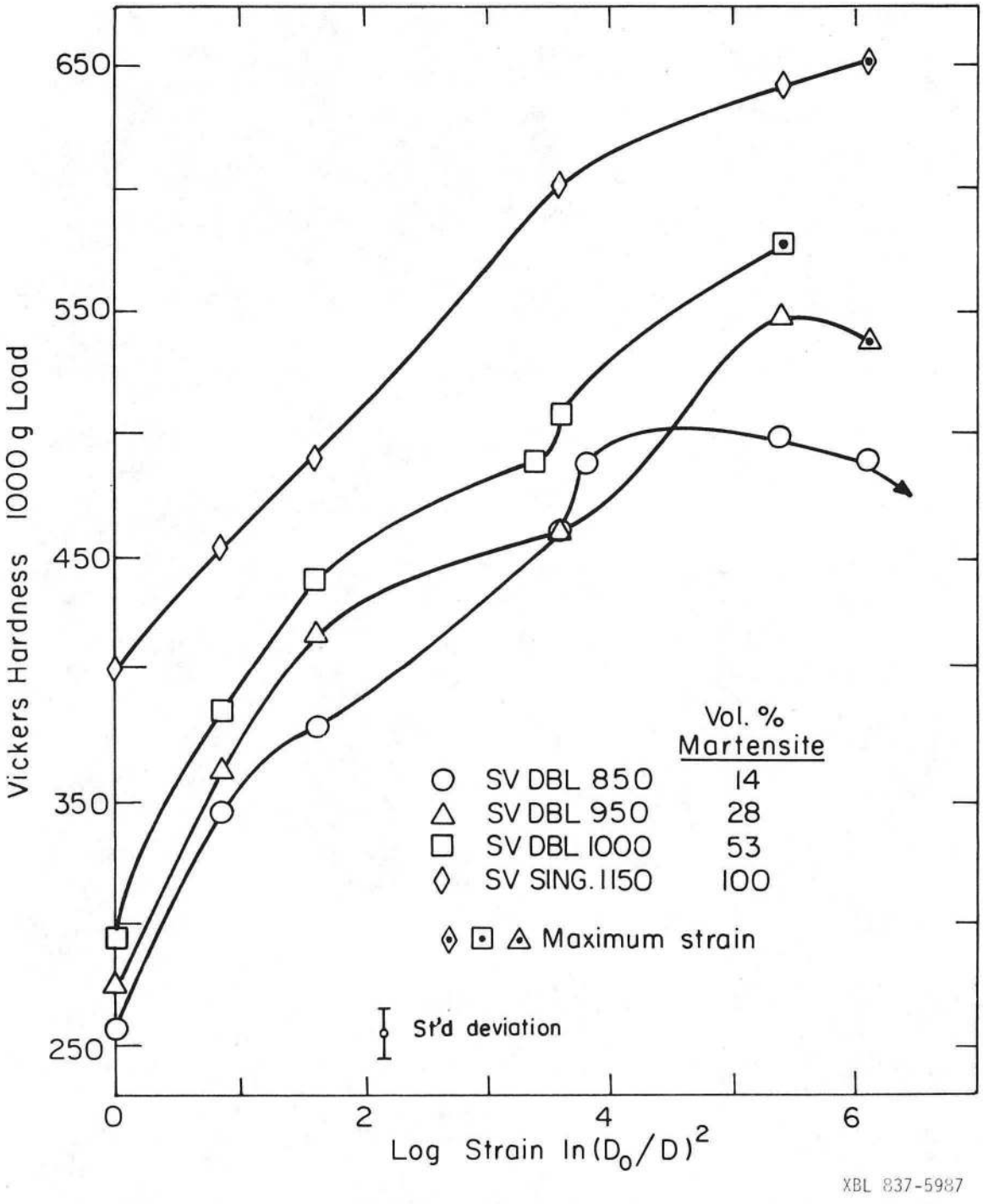
650
550
450
350
250
Vickers Hardness 1000 g Load
0
2
4
6
Log Strain $\ln(D_0/D)^2$
Vol. %
Martensite
SV DBL 850 14
SV DBL 950 28
SV DBL 1000 53
SV SING. 1150 100
Maximum strain
St'd deviation
XBL 837-5987

Fig. 17

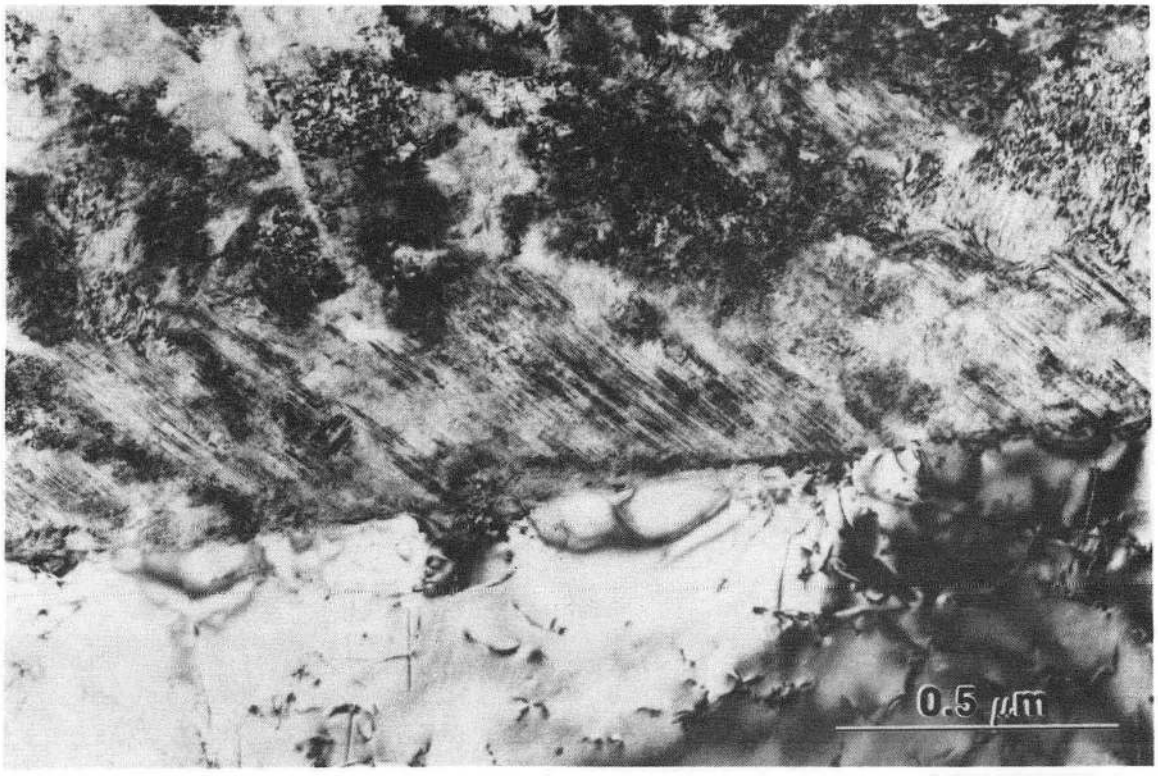

XBB 824-3480

Fig. 18

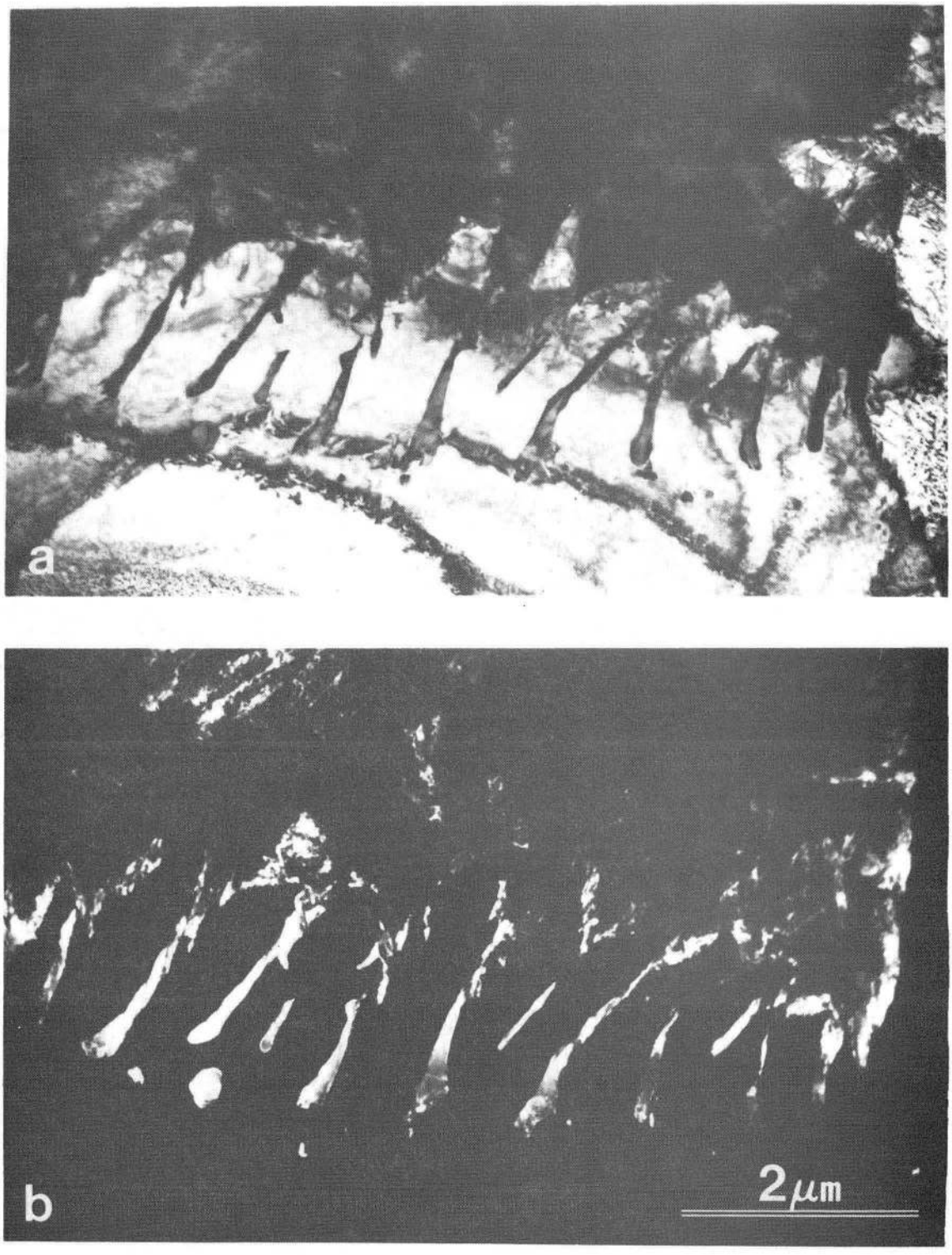

Fig. 19

XBB 837-6003

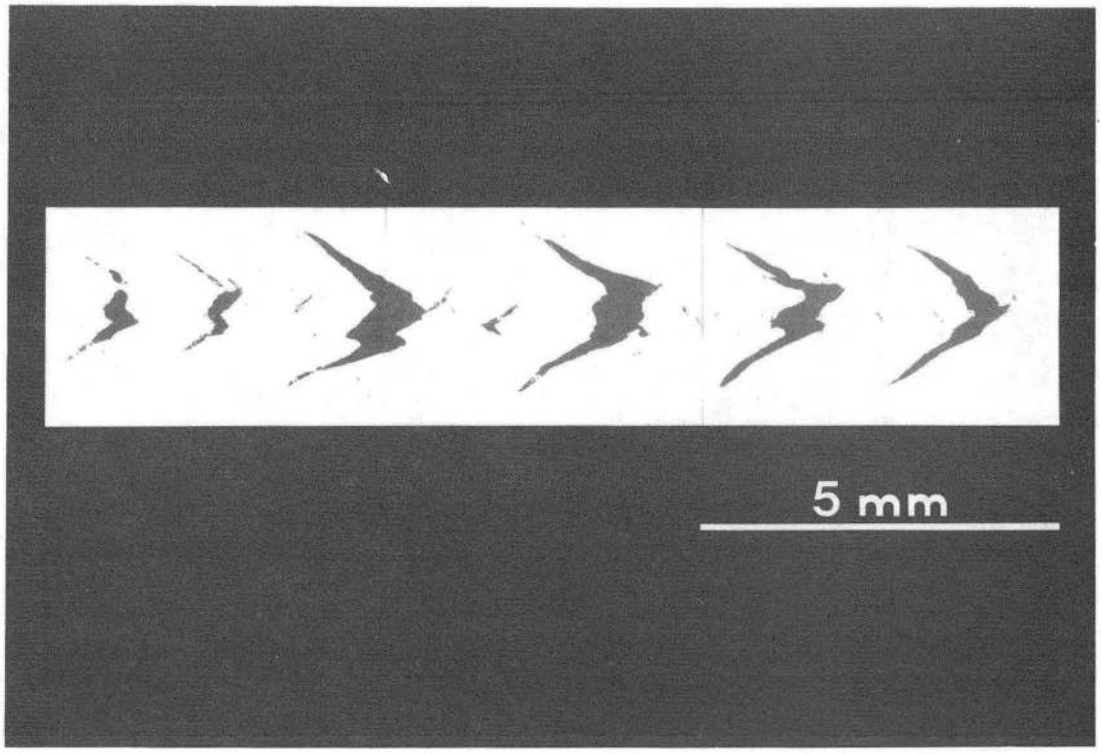

Fig. 20

XBB 829-8597

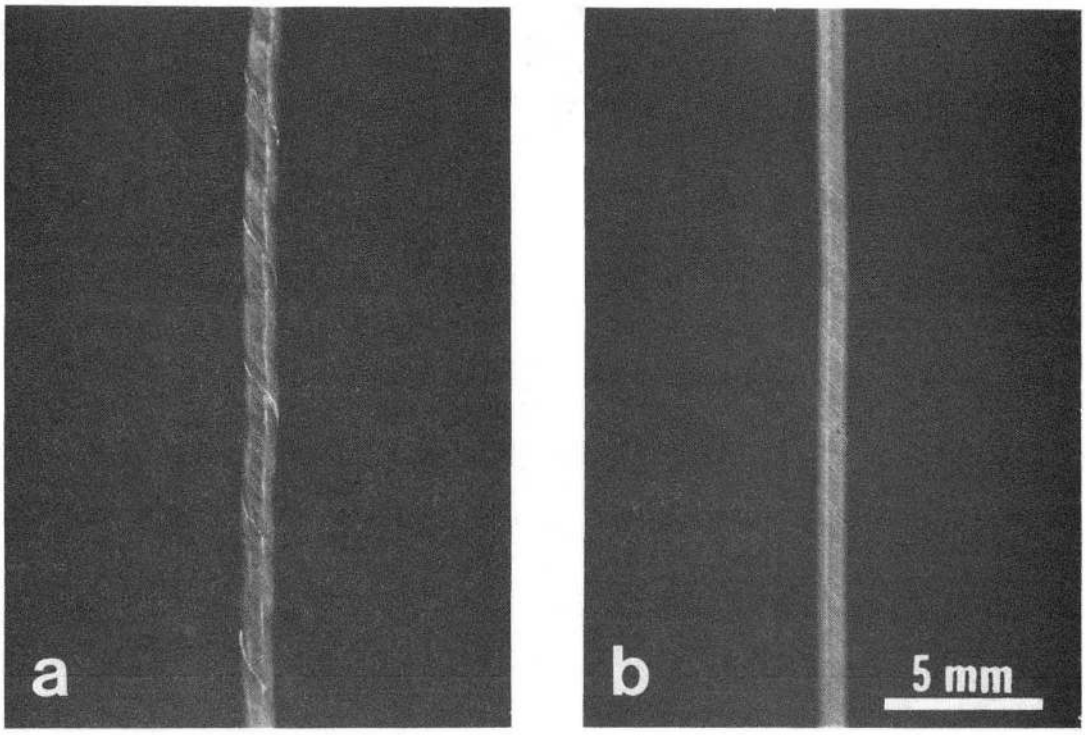

XBB 829-8595

Fig. 21

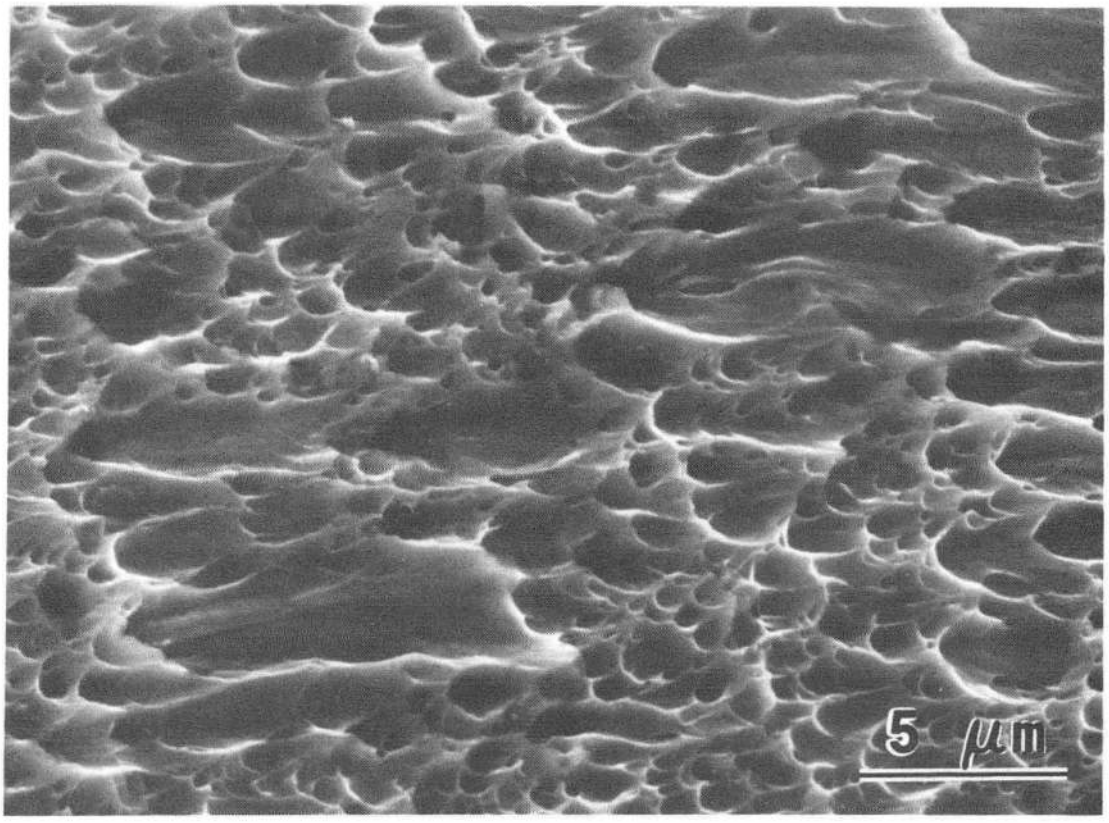

XBB 838-6863

Fig. 22

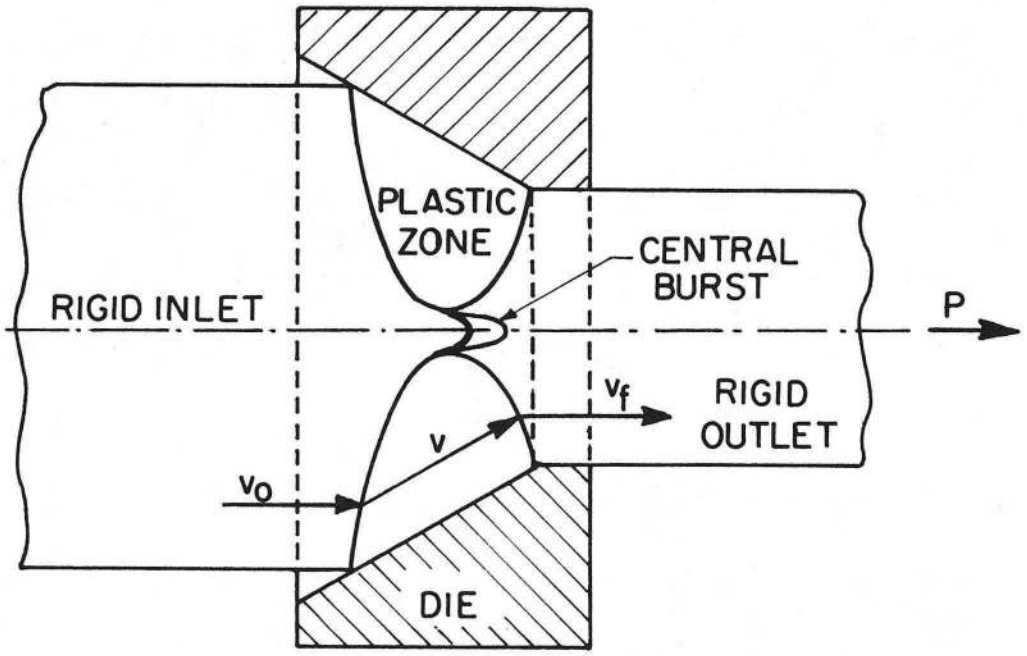

XBL832-5226

Fig. 23

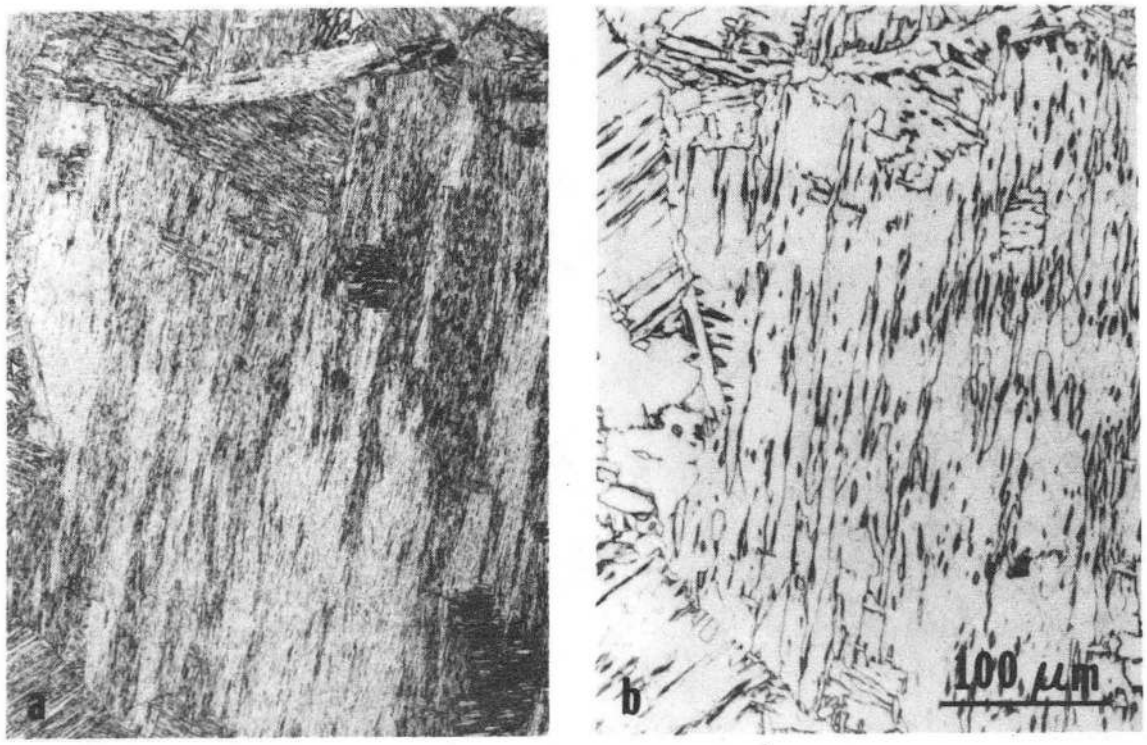

Fig. 24

XBB 820-9788

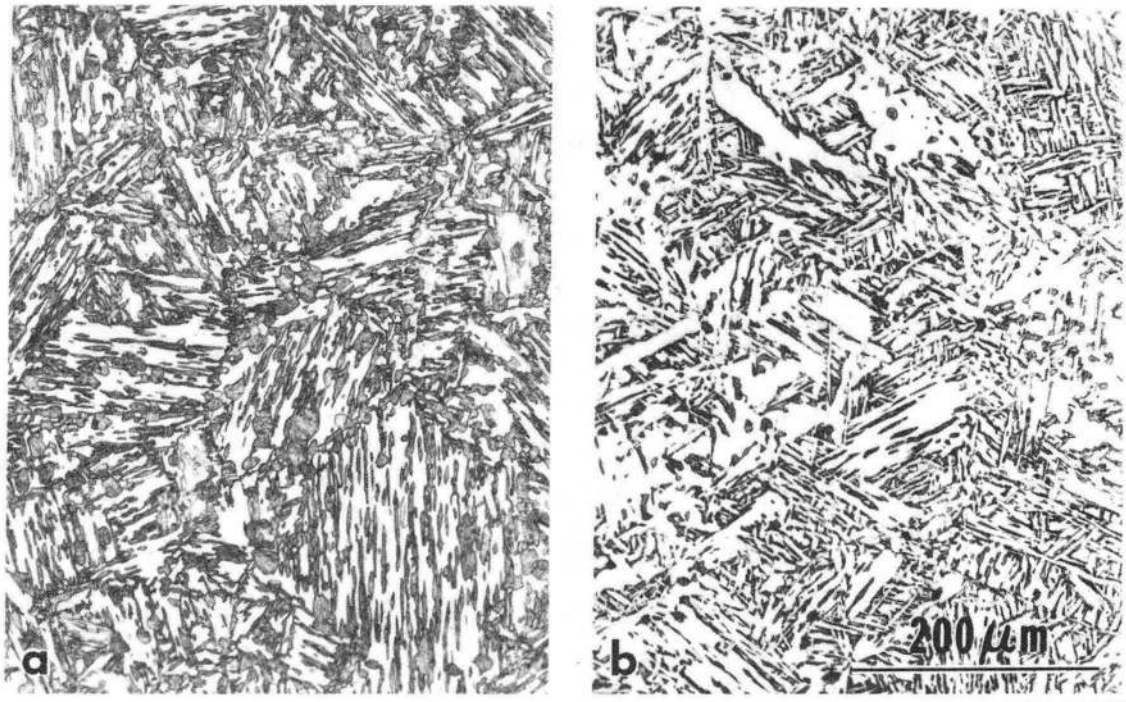

Fig. 25

XBB 838-6864

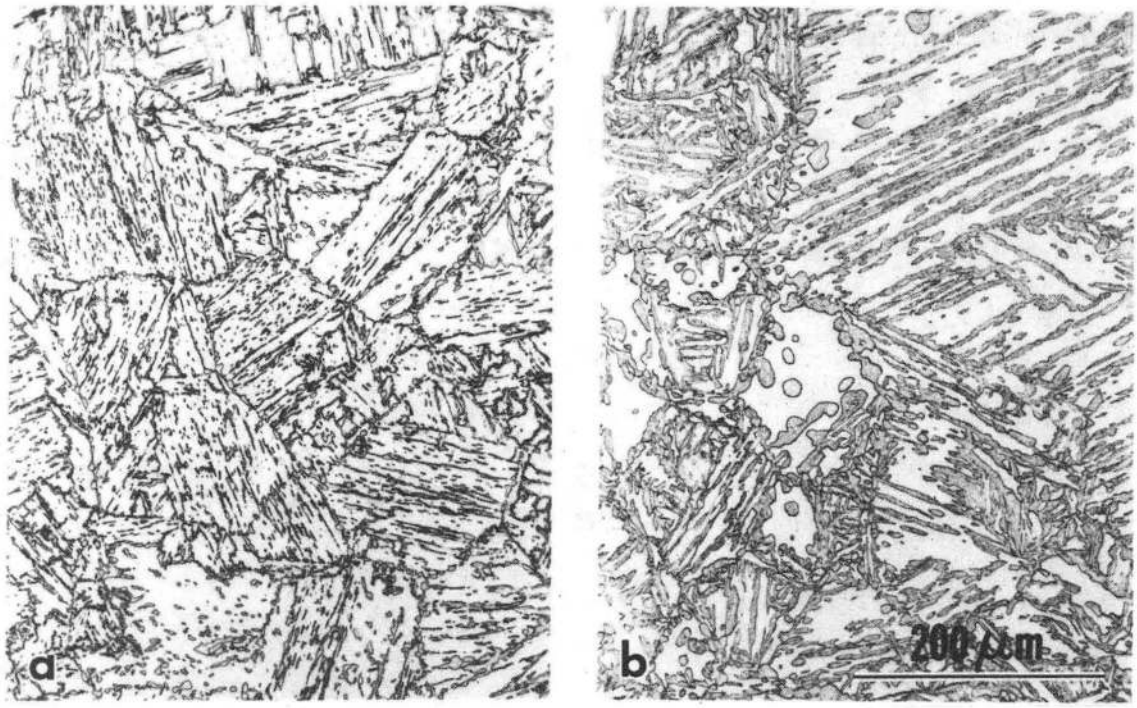

Fig. 26

XBB 837-6008

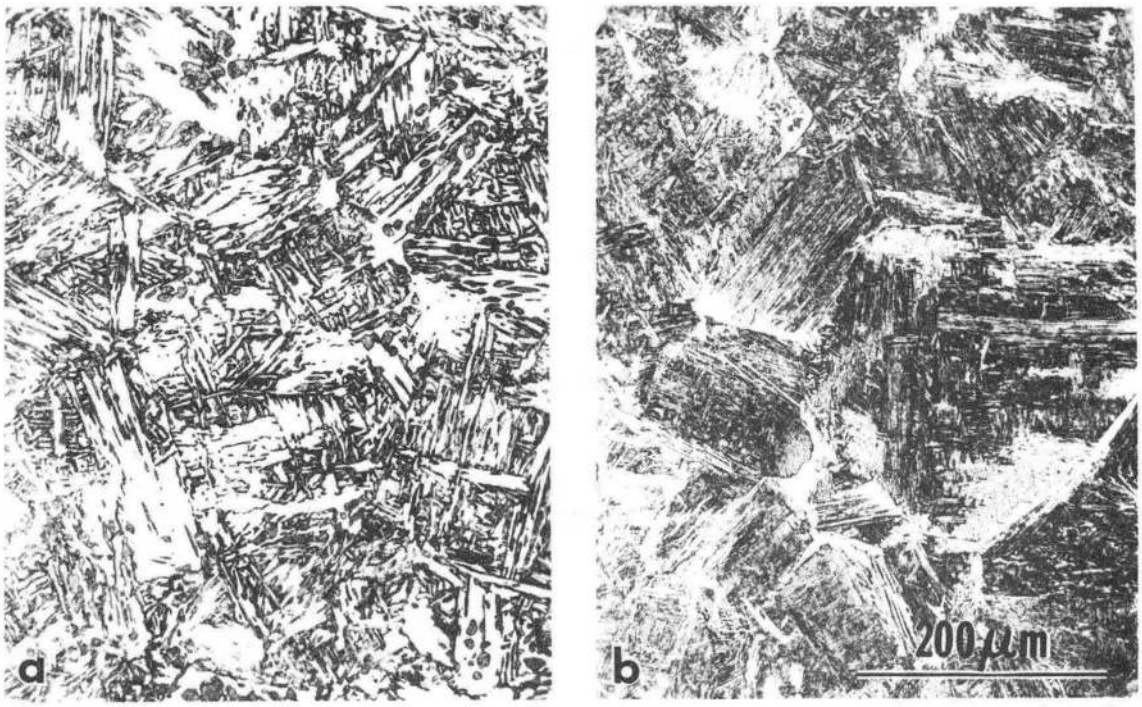

Fig. 27

XBB 837-6006

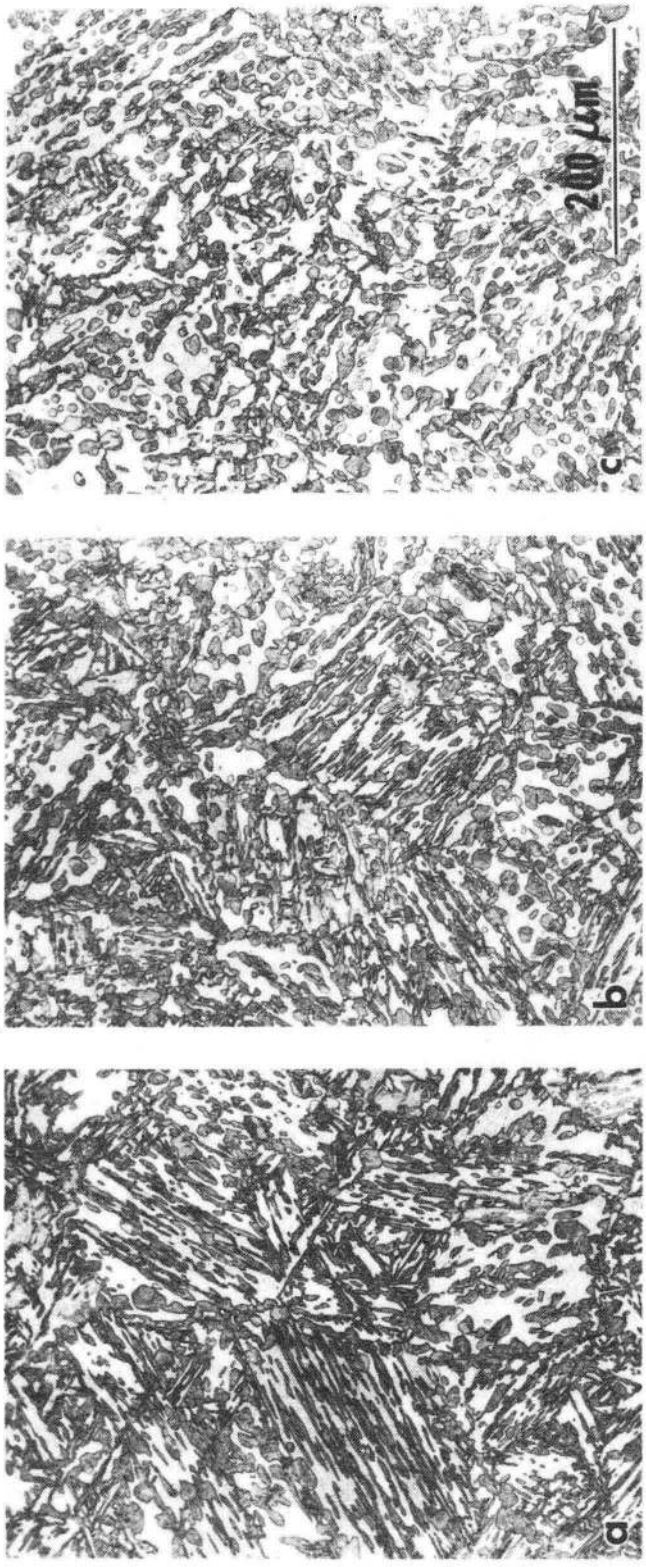

XBB 838-6865

Fig. 28

TECHNICAL INFORMATION DEPARTMENT
LAWRENCE BERKELEY LABORATORY
UNIVERSITY OF CALIFORNIA
BERKELEY, CALIFORNIA 94720